FASE FRONTIERS OF AGRICULTURAL SCIENCE AND ENGINEERING
Engineering Transactions of CAE
REVIEW
2026 / Volume 13 / Issue 3 / 25656

Advancing photocatalytic oxidation process for sustainable treatment of wastewater from livestock production: current breakthroughs and key challenges

Bo SUN[1], Xiaona PAN[2], Xingxing QIAO[1], Wenlong BI[1], Yichen HAO[1], Junmei QIN[1], Qingjie HOU (✉)[1], Fenwu LIU (✉)[1]

1 College of Resource and Environment, Shanxi Agricultural University, Taigu 030801, China.
2 Department of Basic Sciences, Shanxi Agricultural University, Taigu 030801, China.

KEYWORDS

Cost-effectiveness, degradation pathways, modification methods, organic pollutants, visible-light-driven

HIGHLIGHTS

- Adjusting material morphology, particle size and SSA enhances catalytic activity.
- Organic pollutants are degraded by reactive free radicals produced by the catalyst.
- Optimizing energy and material use during synthesis is highlighted.
- Effective use of waste enables circular and low-cost photocatalyst modification.
- Potential approaches for cost control and catalytic applications are outlined.

Received April 26, 2025;
Accepted August 27, 2025.

Correspondences: qingjiehou@163.com, lfwlfw2008@163.com

Special Section: Towards Carbon Neutrality: Advances in Agricultural Production and Emission Reduction (Guest Editor: Hong Yang)

GRAPHICAL ABSTRACT

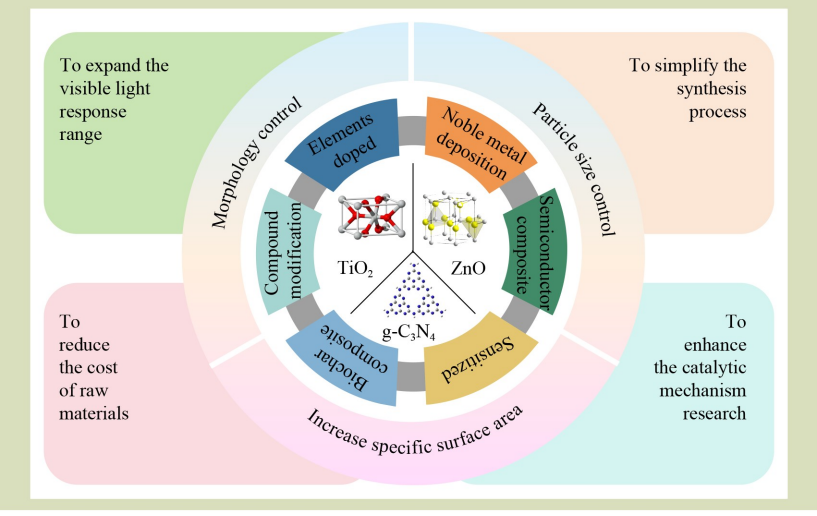

ABSTRACT

Wastewater from livestock production is characterized by a complex composition, high pollutant load and the presence of emerging contaminants. These properties lead to critical challenges in conventional treatment processes, including excessive energy consumption, low treatment efficiency and incomplete pollutant removal. Photocatalytic oxidation is an advanced oxidation process that uses light energy to generate reactive oxygen species to degrade pollutants. It has gained significant attention due to its advantages of high efficiency, environmental friendliness and the ability to mineralize organic pollutants into water, carbon dioxide and other small molecules without consuming fossil energy. However, despite its potential, photocatalytic oxidation has not been widely applied in wastewater treatment. This is mainly

due to the large band gap, low utilization of visible light and fast carrier recombination of photocatalyst. To address these issues, this paper comprehensively reviews the current technical developments of the photocatalytic oxidation process and suggests potentially productive future studies. Despite significant progress, several critical challenges remain to be addressed in photocatalytic material applications, including low visible light utilization, complex synthesis process, expensive material costs, poor practical performance and insufficient mechanism understanding. This review will help design high-efficiency visible-light-driven photocatalysts and promote the application of photocatalysts in the treatment of wastewater from livestock production.

1 Introduction

Large livestock industries discharge substantial amounts of wastewater with high concentration organic pollutants, such as residual veterinary drug antibiotics, antibiotics, pathogens and heavy metals, which are a serious threat to the ecological safety of the surrounding water bodies[1–4]. The metabolites of antibiotics and livestock constantly produce resistant bacteria in the environment and stimulate the dosage of drugs[5,6]. It caused a vicious circle of with drugs contaminating the environment leading to more drug-resistant bacteria that results in increased drug dosage being used and then increased environmental contamination. Due to their hard-degradation nature, these pollutants are inefficiently degraded by conventional processes, and both the pollutants and their degradation intermediates enter water bodies with waste water treatment plants effluent[7]. Given that the vast majority of pollutants are water-soluble, these substances are eventually enriched in the water environment, and then enter the human body through the food chain, causing irreversible toxic operation[8].

Using physical adsorption to remove the organic pollutants from wastewater from livestock production is inefficient[9]. While physical adsorption can temporarily immobilize contaminants through surface interactions, it fundamentally lacks degradation capability, thereby posing risks of secondary pollution from desorption or residual pollutants[10,11]. Also, biological treatment is susceptible to the effect of inhibitory compounds in the wastewater, which can reduce their processing effect[12,13]. Due to physical adsorption and biological treatment processes cannot effectively remove the pollutants in the aquaculture wastewater, the advanced oxidation processes rise in response to the proper time and conditions[14]. These processes are a group of water treatment technologies that use highly reactive oxidizing species to degrade and remove persistent organic pollutants, transforming them into less harmful substances like carbon dioxide and water. These mainly include the Fenton, photocatalytic, ultrasonic and supercritical water processes. Compared with other methods, photocatalytic oxidation shows many advantages, such as simple reaction equipment and safe operation, low cost and high efficiency, and no secondary pollution[15–17]. Since TiO_2 was first used for the photocatalytic degradation of chlorinated biphenyls, semiconductor catalysts, with their highly efficient ability to degrade organic pollutants, have emerged as an emerging technology to address this issue, demonstrating considerable application potential[18–20]. Due to the environmentally friendly semiconductor photocatalyst generating the powerful hydroxyl (·OH) radicals for the oxidative decomposition of organic pollutants only depends on sunlight[21], the photocatalytic oxidation process is favored by an increasing number of researchers[22]. In the process of photocatalytic degradation, organic pollutants are decomposed into non-toxic and harmless inorganic substances, which promotes the sustainable utilization of resources[23–25]. Take TiO_2 as an example, when sufficient light energy irradiates a TiO_2 catalyst, photogenerated e^-/h^+ pairs (with e^- being excited electrons and h^+ positively charged holes) are created between its valence and conduction bands. The h^+ has oxidation capacity and reacts with H_2O to produce ·OH. Meanwhile, the e^- has a reduced capacity and reacts with O_2 adsorbed on TiO_2 in a series of reactions to produce $\cdot O_2^-$ and ·OH.

$$TiO_2+h\nu \rightarrow TiO_2(e^- + h^+) \quad (1)$$

$$h^+ + H_2O \rightarrow \cdot OH \quad (2)$$

$$e^- + O_2 \rightarrow \cdot O_2^- \quad (3)$$

$$\cdot O_2^- + H_2O \rightarrow \cdot O_2H + OH^- \quad (4)$$

$$2 \cdot O_2H \rightarrow H_2O_2 + O_2 \quad (5)$$

$$H_2O_2 + h\nu \rightarrow 2 \cdot OH \quad (6)$$

where, $h\nu$ is a photon.

The photocatalytic oxidation process is extremely effective in degrading organic pollutants, however, several problems limit its application: (1) limited utilization of the solar spectrum[26], so a large amount of visible light energy is wasted (the energy of the visible light used in the photocatalysis process, assuming a wavelength of 420–700 nm, is 2.84×10^{-19}–4.73×10^{-19} J); (2) fast compounding rate of photogenerated carriers[27,28]; (3) to improve catalytic efficiency, photocatalytic materials are usually nanoparticles, which makes them difficult to recycle. Meanwhile, some suspended matter in wastewater from livestock production will lead to deep chroma, which weakens light transmission and will inhibit photocatalytic activity. Therefore, it is necessary to improve the visible light capture ability and photocatalytic activity of photocatalytic materials to promote the photocatalytic oxidation process for wastewater treatment[29]. In addition, semiconductor catalysts also have substantive effects in removing micro-pollutants such as antibiotics and drug residues from water, providing a new approach to solving the problem of micro-pollution in water bodies[30,31].

In recent years, researchers have modified semiconductor catalysts through various methods to enhance their photocatalytic performance. For example, the band gap structure of semiconductor catalysts can be regulated through methods such as ion exchange, doping, recombination and heterojunction construction, thereby enhancing their absorption capacity for visible light[32–34]. This review focuses on the development, application and catalytic efficiency of visible-light-driven TiO_2-based, ZnO-based, and g-C_3N_4-based (in which g is graphite) modified photocatalytic materials, as well as their application costs and prospects. We hope that this review paper can drive the development of highly efficient TiO_2-based, ZnO-based, and g-C_3N_4-based photocatalysts for treatment of wastewater from livestock production.

2 Mechanism of organic matter degradation via photocatalyst process

Most antibiotics in wastewater from livestock production are predominantly the following: tetracyclines, fluoroquinolones, sulfonamides, macrolides, chloramphenicols and β-lactams[35–37]. Photocatalytic degradation can destroy the organic group of antibiotics and convert part of it to CO_2 and H_2O. Given the complexity of organic pollutants and the different photocatalytic materials used, there are different degradation pathways and intermediates even for the same pollutant in the photodegradation process. For example, in the photocatalytic degradation of oxytetracycline, which is a classic tetracycline antibiotic, there are 16 potential photocatalytic intermediates. Based on the charge-to-mass ratio (m/z = 435, 431, 417, 416, 400, 379, 362, 347, 333, 319, 301, 275 and 274), the formulas of intermediates could be obtained, which were presented in Fig. 1[35]. In the TiO_2/Bi_2WO_6/rGO (reduced graphene oxide) photocatalytic degradation of norfloxacin, the h^+ and ·OH are the main reactive oxygen species[36]. With the action of h^+ and ·OH, the norfloxacin is gradually broken down into small molecules of organic matter, mineralized inorganic matter, CO_2, and H_2O (Fig. 2). When it comes to cephalexin (a classic cephalosporin antibiotic), which is widely used in human health and animal agriculture, ZnO nanowires were proven can degrade cephalexin effectively under simulated sunlight[37]. The photocatalytic pathway of cephalexin by ZnO nanowires mainly included hydroxylation, demethylation, decarboxylation and dealkylation, and the specific degradation pathway is shown in Fig. 3.

Dyeing wastewater often has a deep chroma, similar to that of wastewater from livestock production, which can hinder light transmission. Taking the degradation of common azo-dyes as an example, methylene blue (MB) and rhodamine B (Rh B) can be completely degraded in MoS_2@MIL-88(Fe) system to form CO_2, H_2O and other inorganic substances[38]. The mineralization path of MB and Rh B dye was shown in Fig. 4, respectively. Under the action of the N-ethyl group mineralization, the colored C=N bond breaks in the dyes structure, and N-demethylation occur. During N-demethylation, the C–C and C–N bonds of MB and Rh B are cleaved. Active oxidants are heavily involved in the degradation of MB and Rh B, which chemically convert major toxic pollutants into non-toxic secondary products such as water, carbon dioxide, and some mineral salts. Degradation of dyes is achieved by photocatalysts producing hydroxyl (·OH) and

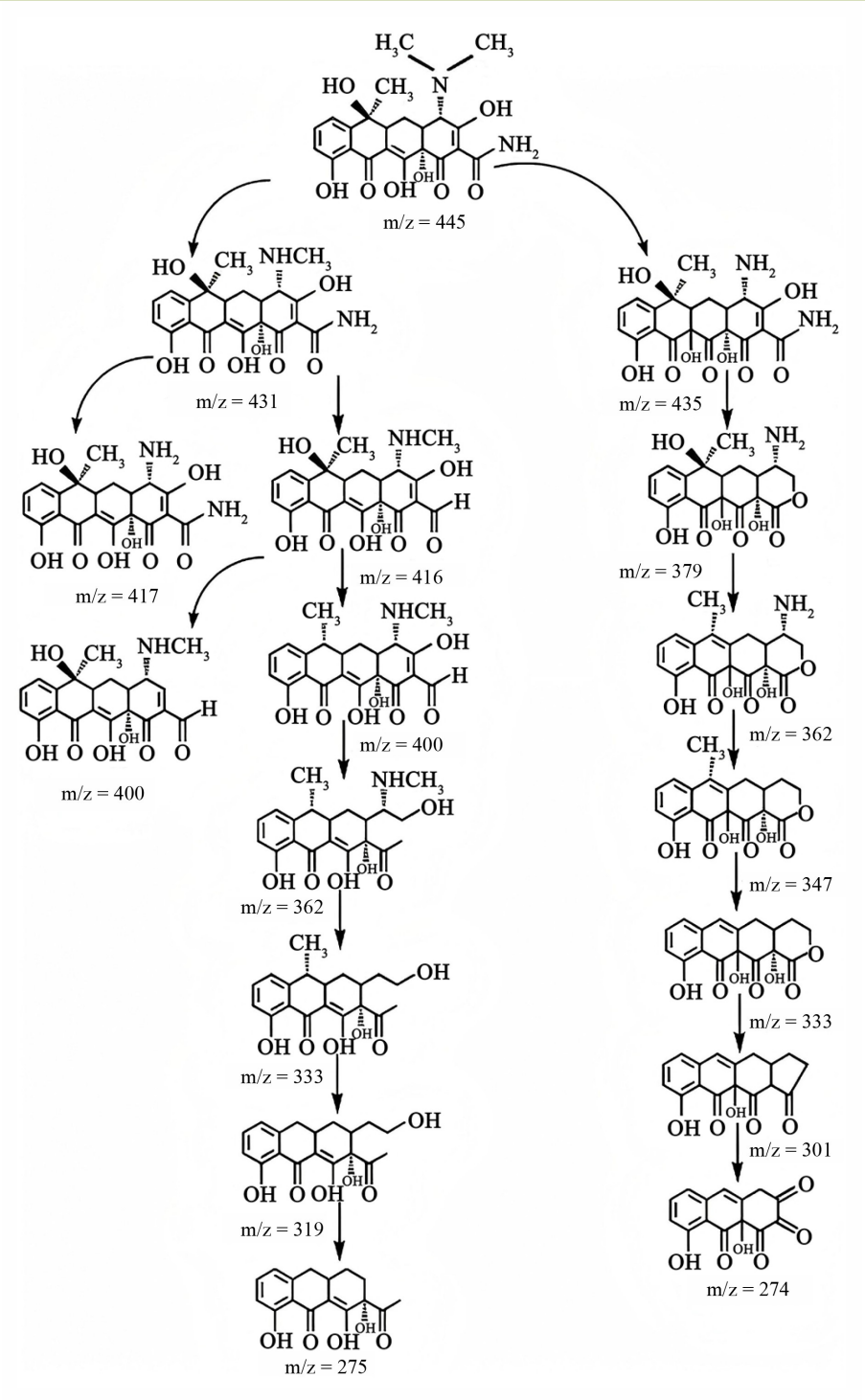

Fig. 1 Proposed pathways of photocatalytic tetracycline degradation. Reproduced from Huang et al.[35], with permission from The Wiley-VCH Verlag GmbH & CO. KGaA.

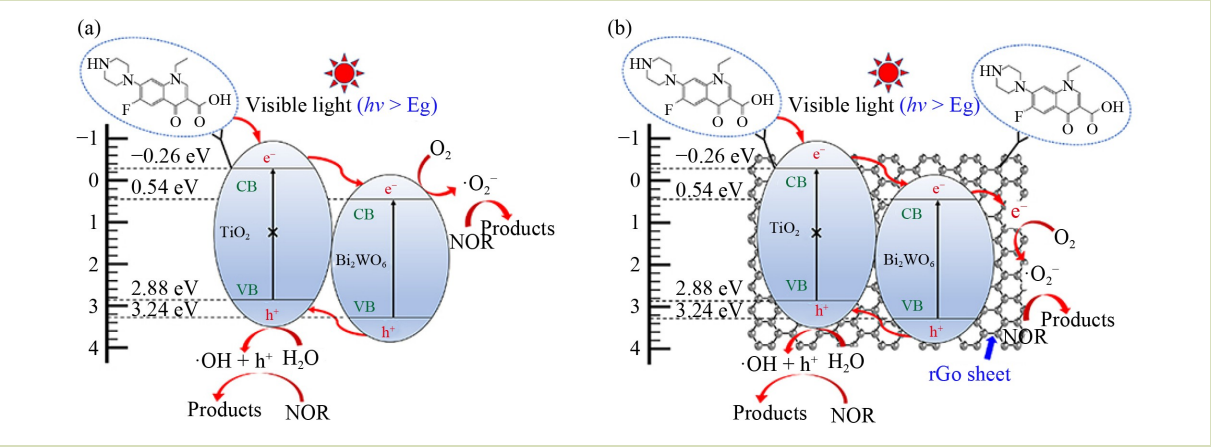

Fig. 2 The possible photocatalytic mechanism of degradation norfloxacin (NOR) by (a) TB and (b) TiO_2/Bi_2WO_6/rGO (reduced graphene oxide) under visible light irradiation. Reproduced from Ma et al.[36], with permission from The Elsevier BV.

superoxide ($\cdot O_2^-$) under light. It can be seen that the modified photocatalyst has a well-catalytic effect even in wastewater with deep chroma.

3 Modification of photocatalysts

3.1 A brief introduction of TiO_2, ZnO and g-C_3N_4 photocatalyst

3.1.1 Titanium oxide

TiO_2 has excellent photocatalytic oxidation ability. For example, it has been reported that TiO_2 can photocatalytically degrade polychlorinated biphenyls, which are known for their hard-to-degrade nature, under UV light[39]. This property has led to its widespread use in the field of photocatalysis, particularly in applications such as converting abundant solar energy into available hydrogen or hydrocarbon energy[40,41], removing CO_2[42] and photocatalytic degradation of organic pollutants[43–46]. However, due to the forbidden band width of TiO_2 being 3.0–3.2 eV, the catalytic reaction can only take place under UV light (λ < 400 nm). As a result, its utilization rate for visible light is extremely low, typically less than 5%[47]. Meanwhile, there is a certain attraction between photogenerated electrons and holes, and some of them recombine on the semiconductor surface, releasing heat instead of free radicals[47]. This recombination process can reduce the quantum efficiency of TiO_2 photocatalysts to below 10%[48]. In this case, the ability of TiO_2 photocatalyst to catalyze the degradation of organic pollutants will be greatly reduced. Therefore, researchers have developed different modification methods to improve the photocatalytic capacity[48].

3.1.2 Zinc oxide

ZnO, with the same band structure as TiO_2, is rich in source, low in price, diversified and adjustable in morphology and has suitable electrical conductivity, thermal conductivity and chemical stability. It is an environmentally-friendly wide-band-gap semiconductor photocatalyst[49–51]. However, the ZnO band gap width of 3.37 eV means its utilization of sunlight is extremely low. For example, its visible light utilization rate is typically < 3%[52]. This limits its light energy utilization efficiency and catalytic activity to a certain extent. The photocatalytic capacity of ZnO remains suboptimal due to rapid electron-hole recombination, with recombination rates as high as 80%[53], and limited visible light absorption[54,55].

3.1.3 Graphitic carbon nitride

g-C_3N_4 is a typical polymer semiconductor with a band gap width of 2.7 eV. It can absorb the solar spectrum wavelength of less than 475 nm blue-violet light[56]. The g-C_3N_4 has an appropriate semiconductor band edge position, which is different from TiO_2 and ZnO. It can effectively activate oxygen molecules and generate superoxide radicals for photocatalytic conversion of organic functional groups and degradation of organic pollutants[57]. Meanwhile, the advantages of low raw material cost, easy synthesis, high stability, unique electronic

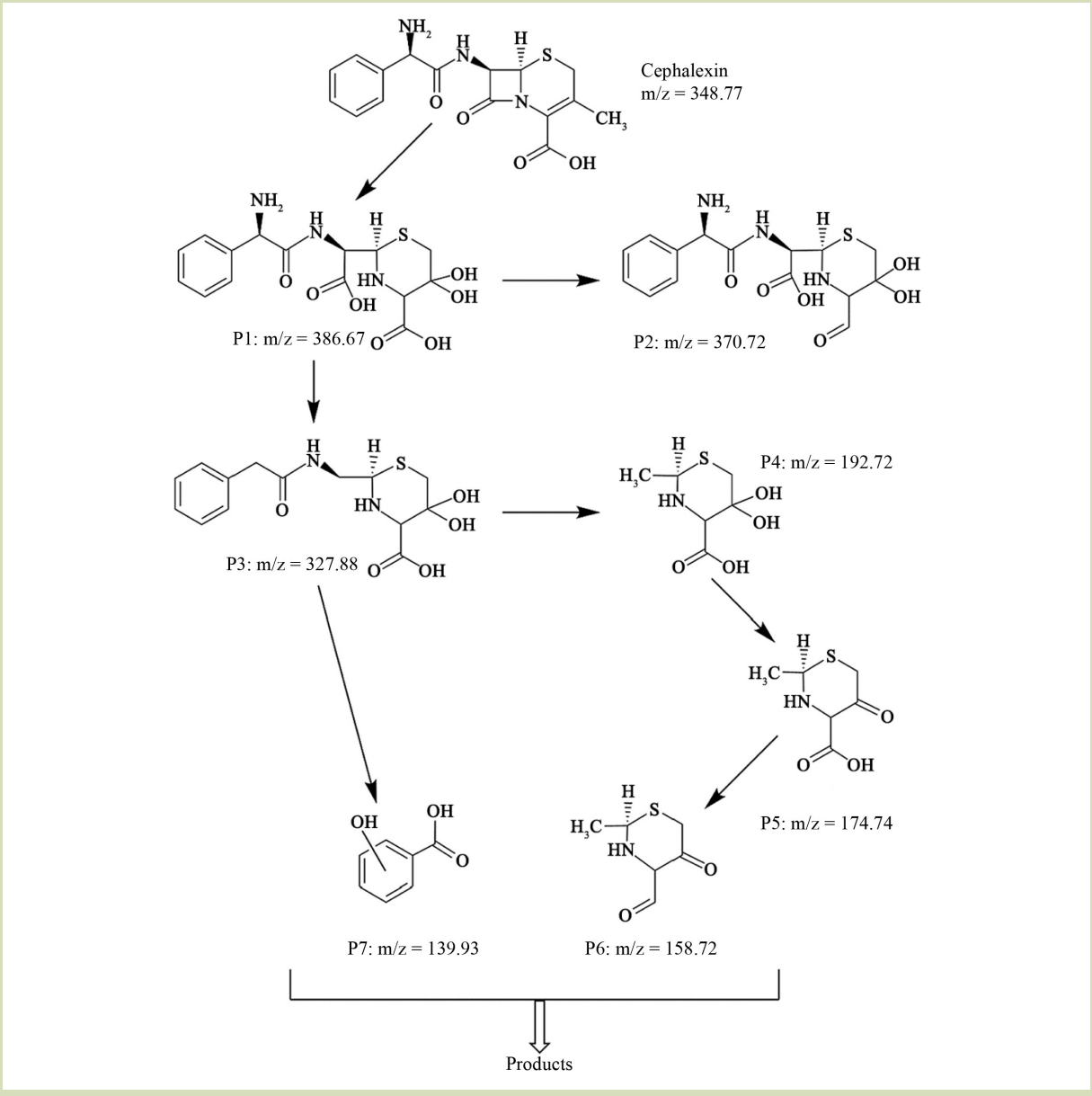

Fig. 3 Proposed photocatalytic degradation pathways of cephalexin by ZnO nanowires under simulated sunlight irradiation. Reproduced from He et al.[37] under Creative Commons.

structure and easy regulation make g-C_3N_4 a promising semiconductor photocatalyst[58]. In addition, g-C_3N_4 has disadvantages such as a low utilization rate of visible light, typically around 10%–15%[59] and a high composite probability of photogenerated electron holes, with recombination rates reaching up to 70%[60]. To improve the performance of g-C_3N_4, a large number of modification studies have been carried out[59,60].

3.2 Photocatalyst modification method

3.2.1 Morphology control

The structure of the photocatalyst itself is often decisive for catalytic efficiency. For example, TiO_2 mainly has three crystal structures anatase, rutile and plate titanium. Of these, the anatase lattice has the most defects and dislocations, which is more conducive to the generation of oxygen vacancy electron

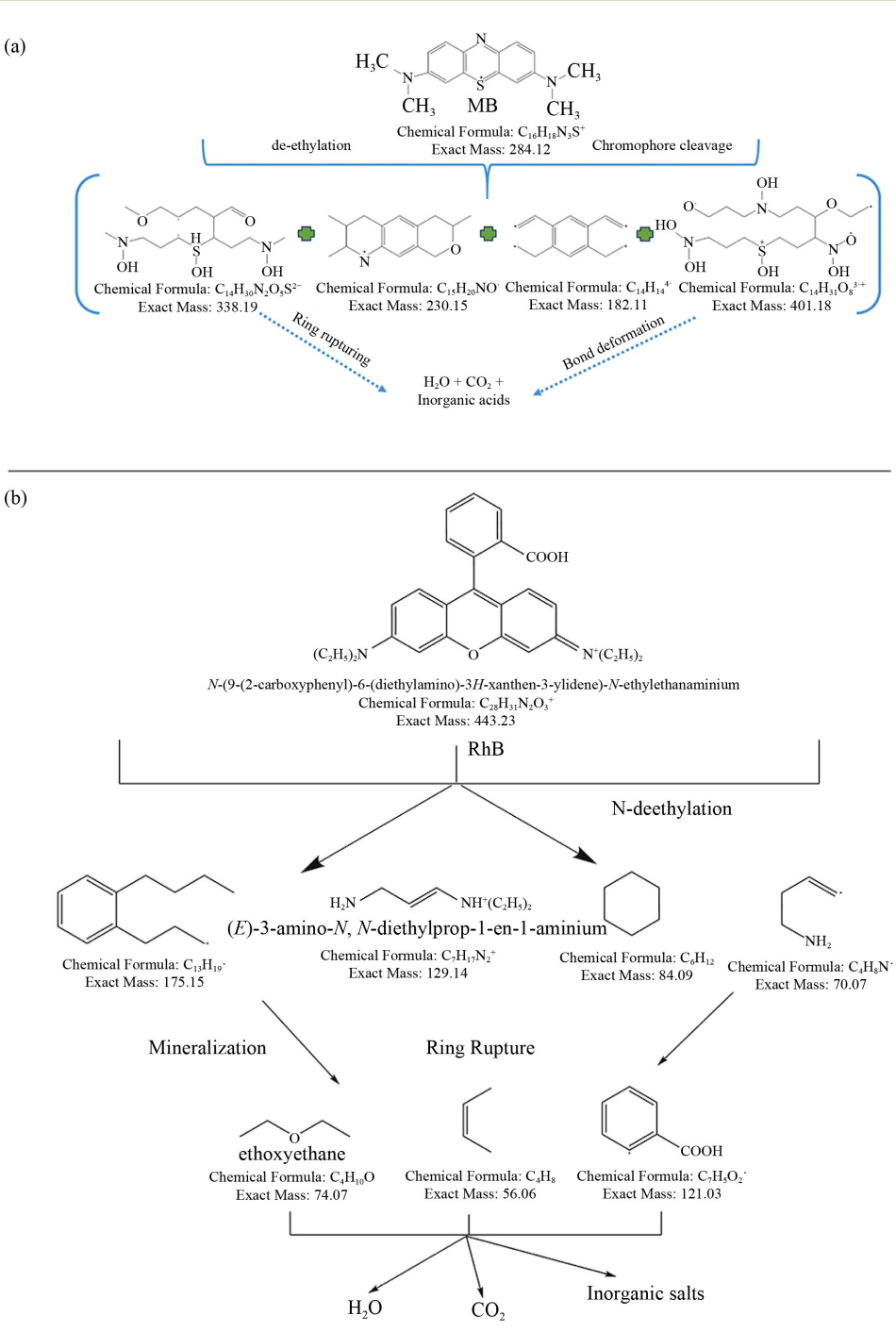

Fig. 4 (a) Proposed degradation pathway of methylene blue (MB) on MoS_2@MIL-88(Fe) catalyst under visible light irradiation, (b) Proposed degradation pathway of rhodamine B (Rh B) on MoS_2@MIL-88(Fe) catalyst under visible light irradiation. Reproduced from Govarthanan et al.[38], with permission from The Elsevier BV.

capture and the inhibition of photoelectron-hole recombination. Therefore, anatase TiO_2 has a higher photocatalytic activity[61]. The mixed crystal structure photocatalytic activity will be higher than that of single crystals when the anatase phase and rutile phase are calcined into TiO_2 mixed crystals in appropriate proportions[62]. The main reason for this is that the crystal structure is equivalent to the composite of two kinds of semiconductors, which promotes the effective separation of photogenerated electrons and holes (Fig. 5).

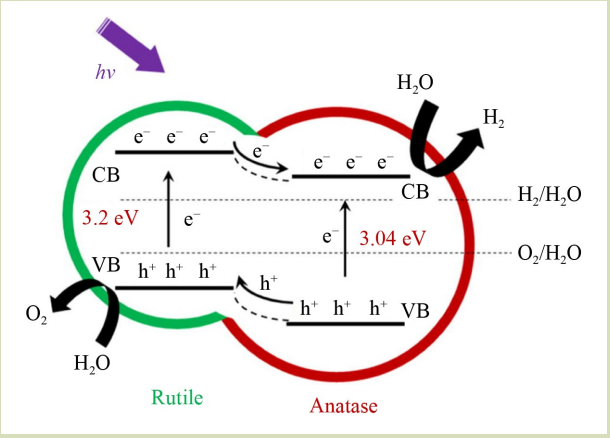

Fig. 5 Photocatalytic overall water splitting mechanism of TiO_2 nanobelts. Reproduced from Jacob et al.[62], with permission from The Academic Press Inc.

The TiO_2 nanoparticles (anatase/rutile mixed crystals) could be used for the degradation of the hazardous dye MB under ultraviolet light illumination[63]. pH1.0-TiO_2, which was synthesized under pH of 1.0, has a rod-like particle morphology and some irregularly shaped particles (Fig. 6). The research result shows that the mixed-phase TiO_2, which was

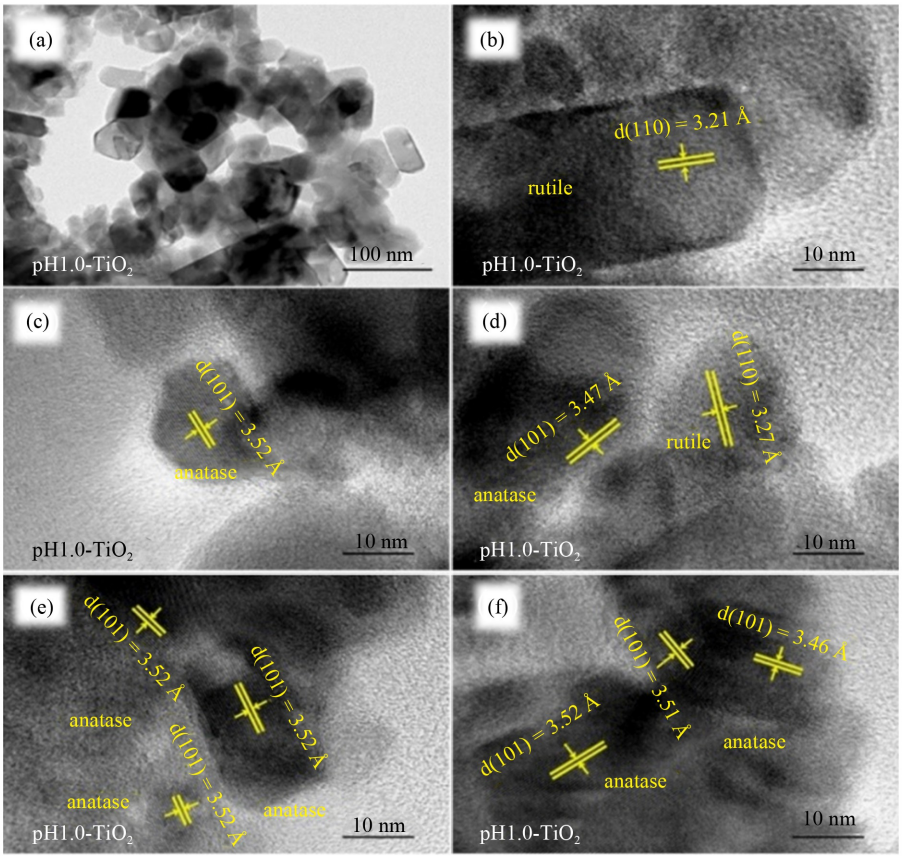

Fig. 6 Transmission electron microscopy (a) and high-resolution transmission electron microscopy (b–f) images of the TiO_2 sample obtained at pH 1.0 under hydrothermal conditions. Reproduced from He et al.[63] under Creative Commons.

synthesized at pH of 1.0, has the highest photocatalytic activity of degradation MB is 85.8% under UV irradiation for 90 min. Compared with pH1.0-TiO_2, the degradation efficiency of the commercial P25 TiO_2 (Nippon Aerosil Ltd., Tokyo, Japan) to MB was only 79.4% under the same light condition.

3.2.2 Particle size control

With the decrease of the semiconductor nanoparticles size, band structure gradually transitions to the energy level structure of atoms or molecules. When the particle size is smaller than the space charge layer thickness, photoproduction carriers from internal migration to the surface more easily. It makes the light born in a semiconductor electron and hole not compound before it has arrived at the surface of the semiconductor, effectively inhibiting the photoproduction of the electronic-hole compound, and improving the quantum efficiency[64,65]. As mentioned above, nano-ZnO can significantly improve the catalytic capacity of ordinary ZnO. This is because the smaller the particle size of photocatalyst nanoparticles, the larger the number of atoms on the surface, the larger the specific surface area, and the higher the light absorption efficiency and adsorption efficiency of the catalyst surface, thus significantly improving the photocatalytic activity of nanomaterials[66–68]. TiO_2 and g-C_3N_4 also have similar properties, which are similar to ZnO. The band gap shifted and carriers migrated to the surface rapidly with the decrease in particle size[69]. When the particle size was as small as 2 nm, there would be an obvious quantum size effect. Using the electrochemical etching process to prepare ultrafine TiO_2 nanoparticles (with an average particle crystal size of 9.87 nm) exhibited high photocatalytic activity, which the photocatalytic degradation efficiency of tetracycline (TC) is 99.4%[70].

The bulk g-C_3N_4 can be etched into nanosheets, which makes the photocatalytic activities significantly enhanced. Scanning electron microscope images confirm that the carbon nitride nanosheets combined with carbon quantum dots (CQDs) are a single-layer nanosheet with jagged edges and lateral dimensions ranging from submicron to several microns (Fig. 7)[71]. In this particular construction, the substrate curvature makes the surface energy of materials minimizes, which enhances the photocatalytic activity of the catalysts.

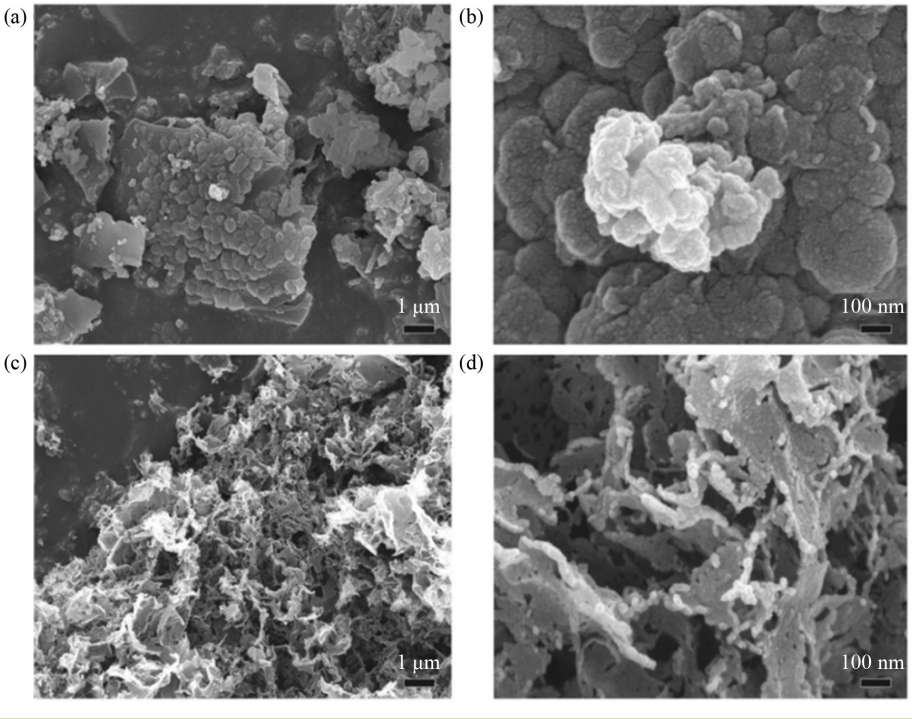

Fig. 7 Scanning electron microscopy images of (a, b) carbon nanobags and (c, d) carbon nitride nanosheets combined with carbon quantum dots. Reproduced from Wang et al.[71], with permission from The Elsevier BV.

3.2.3 Increase specific surface area

The specific surface area of a material is defined as the total surface area of the material divided by its mass or volume. The degradation of organic pollutants by semiconductor photocatalytic oxidation occurs on the surface of the catalyst. With the increase of specific surface area, the formation of photocarriers and the adsorption and transport of reactants and degradation products on the surface are facilitated when other influencing factors, such as lattice defects on the catalyst surface, are the same[72–74]. The optical effect of light sources on the surface of photocatalysts, such as multiple diffraction and diffuse reflection, increases the utilization rate of light and can effectively improve photocatalytic activity. The main ways to improve the specific surface area are the preparation of porous structure materials[75–78], array structure[79,80] and hierarchical structure[81–83].

Anatase TiO_2 with a hollow hexagonal frame structure considerably increases its specific surface area[75]. It is worth noting that the temperature and time of calcination are particularly critical in the process of material synthesis. As shown in Fig. 8(a), when the precursor was calcinated at 100 °C for 2 h, the hexagonal smooth surfaces of TiO_2 crystals begun to disappear. When the calcination temperature was raised to 300 °C, as shown in Fig. 8(b), the side faces of the hexagonal smooth surfaces disappeared and six edges gradually became apparent. However, the side faces of the hexagonal smooth surfaces kept their original morphology. It is easy to see that with the increase of calcination temperature, the TiO_2 crystals gradually grew into hexagonal box structures When the calcination temperature is increased to 600 °C, it can be seen from the scanning electron microscopy image (Fig. 8(c)) that the material remained in hexagonal boxes. When the precursor was calcined (600 °C for 7 h), the prepared TiO_2 with a unique hexagonal framework structure, which has a higher specific surface area (51.9 $m^2 \cdot g^{-1}$) than other calcination conditions. Using this material, with about threefold the surface area of its precursor when calcined at 100 °C for 2 h, increased the removal efficiency of Rh B solution to 98.6% within 40 min. The special array structure can also effectively modify the photocatalytic material. The hexagonal wurtzite nanorod arrays (polyimide/Ag)/ZnO-Ag can be prepared on polyimide, and polyimide/Ag nanofibers by combining electrospinning and hydrothermal reaction processes[80]. The (polyimide/Ag)/ZnO-Ag had improved photocatalytic degradation of MB dye,

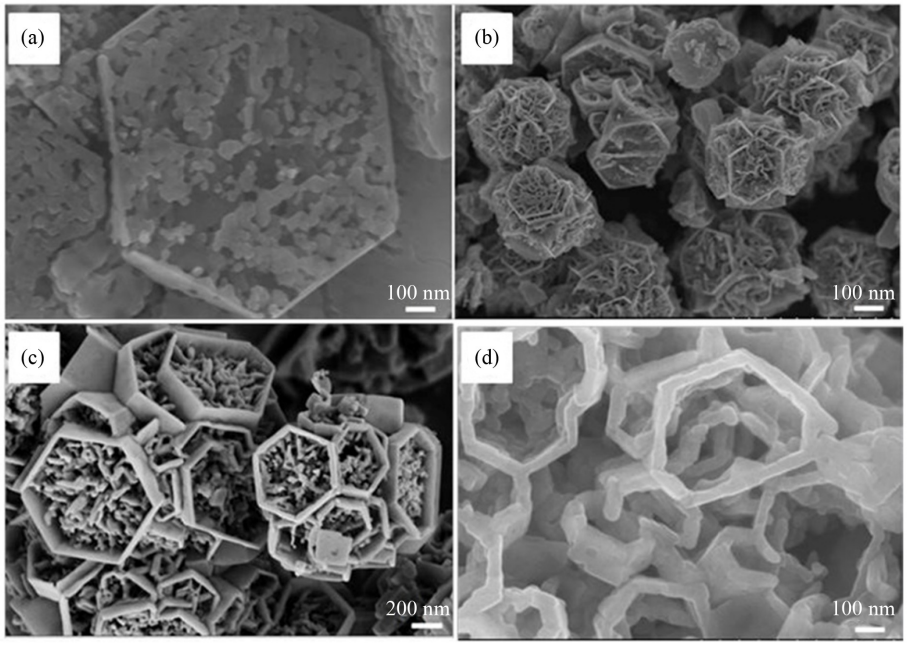

Fig. 8 Scanning electron microscopy images of TiO_2 synthesized with different calcined temperatures: (a) 100 °C for 2 h; (b) 300 °C for 2 h; (c) 600 °C for 2 h; (d) 600 °C for 7 h. Reproduced from Teng et al.[75], under Creative Commons.

with a removal efficiency of 98% under illumination for 120 min.

The ability of g-C_3N_4 with the hierarchical porous structure to degrade organic pollutants is considerable. Using monodisperse SiO_2 as a template, g-C_3N_4 with a graded porous structure can be prepared by simple one-step calcination[81]. The g-C_3N_4 prepared has a specific surface area and visible light absorption performance higher than bulk g-C_3N_4 which helps to facilitate the separation of photogenerated electron holes. The removal efficiency of MO of the catalyst with the best ratio of SiO_2 to dicyandiamide (1:1) reaches 60% within 100 min, which is threefold that of bulk g-C_3N_4. The existence of hierarchical microporous and mesoporous structures can provide additional reaction sites for photocatalytic reactions, which is conducive to enhancing catalytic performance.

3.3 Main modification methods for photocatalysts

3.3.1 Elements-doped

(1) Metal ion-doped

Modification refers to the adjustment of the structure, composition or surface properties of materials through physical or chemical methods to improve their performance. Element doping refers to the introduction of a small number of heterogeneous atoms into materials to alter their electronic structure and physicochemical properties, thereby enhancing the performance of the material.

Metal ions used for semiconductor doping mainly include transition metal ions (Fe^{3+}, Co^{2+} and Cu^{2+}), rare earth metal ions (La^{3+}, Ce^{3+} and Pr^{3+}), and inorganic functional group ions [$Fe(CN)_6^{4-}$ and MoS_4^{2-}], as shown in Table 1. Of these, transition metal ions and rare earth metal ions are the most common[82–87].

TiO_2 nanosheets, with Cu^{2+} doping by solvothermal synthesis, have a high specific surface area and excellent visible light response[82]. By introducing Fe^{3+}, the light absorption range can be further extended from the ultraviolet band to the visible range[83] (Fig. 9). The removal efficiency of Fe^{3+} doped TiO_2 nanotube arrays to methyl orange (MO) was about 1.5 times higher than that of pure TiO_2 nanotube arrays within 120 min. Loading metal ions elements on the surface of nano-ZnO can also provide useful improvement[84–86]. Khan et al.[85] prepared Fe^{3+}/ZnO photocatalytic materials by sol-gel synthesis method. The photocatalytic activity was tested to degrade 4-chlorophenol under visible light, Fe-ZnO of optimum loading proportion had the highest activity, degrading 73% 4-chlorophenol. Another study[86] also found that the Co^{2+} could effectively tune the electronic and optical properties of ZnO in photocatalytic applications. When doped with 3 mol% Co^{2+}, Co^{2+}/ZnO exhibited the best catalytic effect and the degradation efficiency reached 99.7% of direct blue 71 in 150 min. Compared with TiO_2 and ZnO, g-C_3N_4 has a higher activation efficiency for molecular oxygen, which is more conducive to the catalytic degradation of organic pollutants. Under visible light irradiation, the porous Fe^{3+}/g-C_3N_4 can almost complete the degradation of sulfadiazine with a removal efficiency as high as 99.8% within 90 min[87].

(2) Non-metallic elements-doped

In general, doping of non-metallic elements such as C, N, B, S and F positively influences the photography of semiconductors in the visible region[88–95], as shown in Table 2. The

Table 1 Summary of the results for metal ion-doped photocatalyst systems

Photocatalyst and dosage		Optimum doping ratio	Organic pollutant and concentrations	Photodegradation efficiency	Ref.
TiO_2	Cu/TiO_2 (30 mg)	4% Cu doping amount	[TC] = 30 mg·L^{-1}	100 min, over 90%	[82]
	Fe^{3+}/TiO_2 (thin film)	0.2 mol·L^{-1} Fe^{3+} doping	[MO] = 2 mg·L^{-1}	120 min, over 70%	[83]
	Ce/ZnO (150 mg)	–	[RO29] = 10 mg·L^{-1}	50 min, 97.84%	[84]
ZnO	Fe^{3+}/ZnO (800 mg)	0.8% Fe^{3+} doping amount	[4-CP] = 0.6 mg·L^{-1}	60 min, 73%	[85]
	Co^{2+}/ZnO (100 mg)	Co^{2+} ion of 3 mol%	[DB71] = 100 mg·L^{-1}	150 min, 99.7%	[86]
g-C_3N_4	Fe^{3+}/g-C_3N_4 (0.1 mg·L^{-1})	3.2% Fe^{3+} doping amount	[SDZ] = 2 mg·L^{-1}	90 min, 99.8%	[87]

Note: "–", not given in the reference.

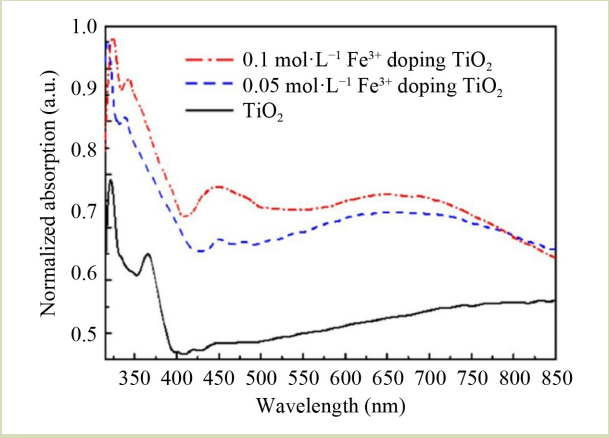

Fig. 9 UV-Vis absorption spectra of pure and Fe^{3+} doped TiO_2 nanotube arrays. Reproduced from Zhang et al.[83] under Creative Commons.

mechanism of improving photocatalyst modification by doping non-metallic elements has not yet been determined. Taking N-doped TiO_2 as an example, the reason can be simply explained as N-doped causes oxygen vacancy and enhances photocatalytic performance. The N-TiO_2 catalyst, obtained after baking in an ammonia atmosphere for 1 h with abundant oxygen vacancies, provides photocatalytic activity 7.59 and 2.26 times higher than pure TiO_2 and the commercial P25 TiO_2 (Evonik Industries)[89], respectively. The N-doped ZnO photocatalyst also has a good photocatalytic effect under visible light. The N-doped ZnO photocatalyst has been synthesized by sol-gel method and photocatalysis experiments show that N-doped ZnO has a significant enhancement of degradation for MB under irradiation of both UV and visible light region[91]. Similarly, N self-doping enhances the utilization of visible light by g-C_3N_4 nanosheets, promotes photogenerated electron-hole separation, and prolonged the lifetime of photogenerated charge carriers[94,95]. As N atoms occupy oxygen vacancies, the band gap width of the photocatalytic material was reduced and the motion of photogenerated electrons was accelerated, which in turn facilitates the photocatalytic reaction.

3.3.2 Noble metal deposition

The photocatalytic reaction takes place on the semiconductor surface, so its surface structure has a considerable influence on photocatalytic performance. Noble metals have higher corrosion resistance and oxidation resistance, which enables photocatalysts remain stable during the catalytic process. In addition, the deposition of noble metal on the surface of photocatalytic material can change the surface properties of the catalyst and the electron distribution of the system, to improve the photocatalytic performance[96–101], as shown in Table 3.

Ag has excellent electrical conductivity, so it is often used as a noble metal element in modified photocatalysts. Podasca and Damaceanu[98] synthesize hybrid polymer films loaded with ZnO-Ag particles and explore their photocatalytic removal efficiency of MO. Its degradation efficiency for MO peaked at 95% when a hybrid film was loaded with 5% ZnO-Ag particles. Due to the synergistic effect between noble metals, the deposition of two noble metals tends to provide better modification of photocatalytic materials. Lee et al.[100] prepared ZnO nanocomposites modified with bimetallic Au and Pd nanoparticles by polylactic acid technique and photodeposition

Table 2 Summary of the results for non-metallic elements-doped photocatalyst systems

Photocatalyst and dosage		Optimum doping ratio	Organic pollutant and concentrations	Photodegradation efficiency	Ref.
TiO_2	S/TiO_2 (30 mg)	S^{4+}/S^{6+} ratio of 1:5.5	[CIP] = 10 mg·L^{-1}	140 min, 91.5%	[88]
	N/TiO_2 (50 mg)	1 h in an NH_3 atmosphere	[TC] = 20 mg·L^{-1}	10 min, over 80%	[89]
	C/TiO_2 (100 mg)	2 atoms% of carbon	[MB] = 20 mg·L^{-1}	120 min, over 90%	[90]
ZnO	N/ZnO (10 mg)	2 h under N_2 atmosphere	[MB] = 10 mg·L^{-1}	180 min, 80%	[91]
	S/ZnO (100 mg)	0.5 wt% S-doped	[Rh B] = 5 mg·L^{-1}	90 min, 100%	[92]
g-C_3N_4	Cl/g-C_3N_4 (50 mg)	NH_4Cl to melamine is 1:1	[TC] = 10 mg·L^{-1}	120 min, 92%	[93]
	N/g-C_3N_4 (50 mg)	–	[TC] = 10 mg·L^{-1}	60 min, 81.72%	[94]
	N/g-C_3N_4 (100 mg)	N to CN is 2 mg:1 g	[Phenol] = 10 mg·L^{-1}	180 min, 70.1%	[95]

Note: "–", not given in the reference.

Table 3 Summary of the results for noble metal deposition photocatalyst systems

Photocatalyst and dosage		Optimum doping ratio	Organic pollutant and concentrations	Photodegradation efficiency	Ref.
TiO_2	Pd/TiO_2 (8 mg)	0.5 wt% of Pd	[PCB 3] = 0.2 mol·L^{-1}	30 min, 100%	[96]
	Ag/TiO_2 (25 mg)	5% of 30 nm Ag	[TC] = 10 mg·L^{-1}	90 min, 90%	[97]
ZnO	Ag/ZnO (1 g)	5 wt% of Ag	[MO] = 1×10^{-3} mol·L^{-1}	250 min, 95.17%	[98]
	Nd-V-ZnO (180 mg)	Nd (4 mol%) and (1 mol%) V	[MO] = 10 mg·L^{-1}	150 min, 99.3%	[99]
	Au/Pd/ZnO (0.5 mg)	Au 15 wt% and Pd 5 wt%	[MB] = 5.0×10^{-4} mol·L^{-1}	180 min, 97%	[100]
g-C_3N_4	Au/g-C_3N_4	1 wt% of Au	[Paracetamol] = 0.3 mg·L^{-1}	25 min, 100%	[101]

method, and the ZnO/Au/Pd nanocomposite removal efficiency of MB was about 5.4 times than pure ZnO.

Although noble metal deposition can considerably enhance photocatalytic performance, inevitably increasing the raw material cost of preparing photocatalytic materials, it greatly restricts the development and application of this kind of material. The search for substitutes is extremely necessary. There are several non-noble metal alternatives that have shown promising performance for specific pollutants. Copper has been frequently investigated as an alternative to rare metal materials, especially in catalysis. For example, Cu-based nanomaterials have demonstrated excellent catalytic efficiency in the oxidation and decomposition of organic pollutants, providing cost-effectiveness far superior to that of precious metal catalysts[102]. Also, a Cu/TiO_2 composite has been reported to have excellent activity in the degradation of organic pollutants[103]. Also, Mo, having an elemental abundance that lies between that of the non-noble and the noble metals and a price comparable to that of non-noble metals, has been examined a an alternative to noble metals[104,105]. For example, MoS_2 nanoflowers have provided suitable photodegradation performance for various pollutants[106]. In terms of photocatalysts, two-dimensional materials, carbon-based quantum dots and Mxenes are emerging as promising alternatives.

3.3.3 Semiconductor composite photocatalysts

Semiconductor compositing is a common modification method to improve the photocatalytic capacity. By combining two or more materials under the premise of an appropriate energy band to modify the photocatalyst, the composite material not only effectively adjusts the performance of a single material, but also generates many new photochemical and physical properties. Binary compound semiconductors, for example, with two types of semiconductor compounds of different band structure, have potential differences that promote the separation of electron-hole pair[107–123] (Table 4).

Combining the two kinds of semiconductors to form semiconductor composite photocatalysts can also improve visible light utilization. The MoS_2@TiO_2 nanosheet heterojunction composite material was used for photocatalytic degradation of MB, with highest removal efficiency of 86% within 180 min, which is much greater than that of pure TiO_2[107]. When the two semiconductors are compounded, their energy band structure is also changed, which improves the absorption and utilization of visible light and decreases the compounding rate of the photogenerated electron-hole. One study[109] also found that $SnIn_4S_8$ nanosheet/TiO_2 hollow sphere heterojunction has high photocatalytic efficiency. When the addition of $SnIn_4S_8$ increases, the light absorption range of the $SnIn_4S_8$/TiO_2 heterostructure broadens toward the visible band, which means that the addition of $SnIn_4S_8$ helps to enhance the absorption of visible light by TiO_2. The $NaBiS_2$ is a narrow-band-gap semiconductor. When it is combined with a wide-band-gap semiconductor, like ZnO, it can enhance the oxidation ability and photocatalytic activity[112]. $NaBiS_2$/ZnO nanocomposites provide greater photocatalytic ability than pure $NaBiS_2$ and ZnO. The removal efficiency of the optimal ratio $NaBiS_2$/ZnO nanocomposite for Rh B is 99% under visible light irradiation within 120 min. The transfer of photogenerated electrons through the interface between $NaBiS_2$ and ZnO slows down the compounding rate of electron-hole pairs, which improves the efficiency of photocatalysis. The g-C_3N_4-based composite photocatalysts have a strong photocatalytic capacity for organic pollutants in wastewater under visible light. One study[121] has reported that CoP as a co-catalyst modified g-C_3N_4 (HCCN) to form a stable

Table 4 Summary of the results for semiconductor composite photocatalyst systems

Photocatalyst and dosage		Optimum doping ratio	Organic pollutant and concentrations	Photodegradation efficiency	Ref.
TiO_2	MoS_2/TiO_2 (A thin film)	–	[MB] = 5 mg·L^{-1}	180 min, 86%	[107]
	Black anatase-TiO_2 (20 mg)	–	[TC] = 10 mg·L^{-1}	270 min, 66.2%	[108]
	$SnIn_4S_8/TiO_2$ (20 mg)	5 wt% of $SnIn_4S_8$	[MO] = 15 mg·L^{-1}	60 min, 90.1%	[109]
	$Bi_2WO_6@TiO_2$ (10 mg)	–	[MB] = 10 mg·L^{-1}	70 min, 96%	[110]
	$CoFe_3O_4@TiO_2$ (5 mg)	–	[MB] = 100 mg·L^{-1}	60 min, 91%	[111]
ZnO	$NaBiS_2$/ZnO (10 mg)	$NaBiS_2$/ZnO is 10:1	[Rh B] = 50 mL	120 min, 99%	[112]
	$Bi_{24}O_{31}Br_{10}$/ZnO (50 mg)	5 wt% of $Bi_{24}O_{31}Br_1$	[Rh B] = 10 mg·L^{-1}	40 min, 92%	[113]
	Ag_8S/ZnO (50 mg)	–	[Rh B] = 1 × 10^{-2} mol·L^{-1}	120 min, over 90%	[114]
	$AgIO_4$/ZnO (100 mg)	15 wt% of $AgIO_4$	[IC] = 5 × 10^{-5} mol·L^{-1}	180 min, 88%	[115]
	g-C_3N_4/ZnO (25 mg)	–	[Crystal violet] = 20 mg·L^{-1}	180 min, 97%	[116]
g-C_3N_4	$CuInS_2$/g-C_3N_4 (50 mg)	50 wt% of $CuInS_2$	[TC] = 20 mg·L^{-1}	60 min, 83.7%	[117]
	$Bi_4O_5I_2$/g-C_3N_4 (100 mg)	–	[MO] = 20 mg·L^{-1}	40 min, 99.96%	[118]
	$Bi_7O_9I_3$/g-C_3N_4 (50 mg)	mass ratio of Bi $(NO_3)_3$·$5H_2O$/g-C_3N_4 is 12.125	[DOX] = 20 mg·L^{-1}	120 min, 80%	[119]
	WO_3/g-C_3N_4 (50 mg)	–	[TC] = 20 mg·L^{-1}	120 min, 90.54%	[120]
	CoP/g-C_3N_4 (40 mg)	5 wt% of CoP	[TC] = 10 mg·L^{-1}	120 min, 96.7%	[121]
	SnO_2/g-C_3N_4 (50 mg)	3 wt% of SnO_2	[TC] = 30 mg·L^{-1}	120 min, 95.90%	[122]
	$CoFe_2O_4$/g-C_3N_4 (200 mg)	3 wt% of $CoFe_2O_4$	[4-CP] = 1 × 10^{-3} mol·L^{-1}	240 min, about 50%	[123]

Note: "–", not given in the reference.

and highly efficient CoP/HCCN composite via a simple solvothermal method. The semiconductor composite photocatalyst provided highly efficient catalytic degradation of TC. With CoP/HCCN of 5 wt% of CoP, TC was degraded by 96.7% within 120 min, which was 10.2 times higher than the degradation efficiency of TC by HCCN.

Although semiconductor composite photocatalysts provide suitable catalytic performance and controllable cost, the narrow-band-gap semiconductors which are matched with TiO_2, ZnO and g-C_3N_4 are often toxic, difficult to prepare, or unstable and prone to photo corrosion. Therefore, further development of low-cost, non-toxic, and harmless narrow-band-gap semiconductors is key to promoting the large-scale application of semiconductor composite photocatalysts.

3.3.4 Dye-sensitized and quantum dot-sensitized

Dye-sensitized and quantum dot-sensitized are new methods to improve visible light catalytic degradation of organic pollutants with TiO_2, ZnO and g-C_3N_4-based photocatalysts[124–128]. Table 5 shows several common dye-sensitized and quantum dot-sensitized methods reported in recent years.

Dyes adsorbed on semiconductor surfaces can absorb all visible light and even near-infrared light. As visible light is absorbed by dye, the electrons on the dye will jump from the ground state to the excited state. When the potential of the free electrons generated by the excited dye is higher than the potential of the photocatalytic materials conduction band, the electrons on the dye will be transferred to the semiconductor. Using organic dye D35 sensitized TiO_2 nano-crystalline film to form a high-efficient visible-light photocatalyst, which has over 85% degradation efficiency of bisphenol A (BPA) within 180 min[124]. The study also found that using chlorophyll sensitized TiO_2 nanoparticles photocatalytic can efficiently degrade MB under visible light, which optimum removal efficiency was 85% within 2 h[125]. The key to dye-sensitized lies in the rapid injection of excited electrons into the semiconductor photocatalyst, and avoiding the recombination of excited electrons and dye positive ions free radicals.

Table 5 Summary of the results for dye-sensitized and quantum dot-sensitized photocatalyst systems

Photocatalyst and dosage		Optimum doping ratio	Organic pollutant and concentrations	Photodegradation efficiency	Ref.
TiO_2	D35 Dye-sensitized/TiO_2 (8 mg)	0.1 mmol·L^{-1} D35-dye	[BPA] = 5 mg·L^{-1}	180 min, over 85%	[124]
	chl Dye-sensitized/TiO_2 (250 mg)	0.1 wt% of chl	[MB] = 20 mg·L^{-1}	120 min, 85%	[125]
	CQDs/TiO_2 (4 mg)	Weight ratio of 1:10 of CQD and TiO_2	[MO] = 20 mg·L^{-1}	180 min, over 80%	[126]
g-C_3N_4	CQDs/g-C_3N_4 (10 mg)	with CQDs stock solution 50 μL	[DCF] = 10 mg·L^{-1}	60 min, 100%	[127]
	BPQDs/g-C_3N_4 (30 mg)	–	[OTC and Rh B] = 10 mg·L^{-1} [TC] = 20 mg·L^{-1}	60 min, 81.05% (OTC) 20 min, 99.43% (Rh B) 60 min, 77.11% (TC)	[128]

Note: "–", not given in the reference.

Quantum dots are nanoscale semiconductors, and the principle of quantum dot-modified photocatalyst is to use light energy to excite the electrons on the surface of carbon quantum dots to form electron-hole pairs, thus promoting the photocatalytic reaction process[126–128]. CQDs are zero-dimensional, fluorescent carbon-based nanomaterials, typically smaller than 10 nm in size with a substantial percentage of oxygen and hydrogen atoms on their surface, which gives them low toxicity and excellent biocompatibility. CQD sensitizing is a promising way to enhance the efficiency of degraded organic pollutants of photocatalysts under visible light. CQD/TiO_2 provides high-efficiency MO photodegradation in direct sunlight exposures, which the optimized doping ratio in the weight ratio of CQD and TiO_2 (threefold the activity of pure TiO_2)[126]. The CQD modified g-C_3N_4 with optimal CQDs loading exhibits extremely high photocatalytic efficiency, which has 15 times the removal efficiency to diclofenac higher than that of pure g-C_3N_4[127]. In addition to CQDs, BPQDs can also have the same effect. The tubular g-C_3N_4 with BPQDs has unusual photocatalytic efficiency in the degradation of oxytetracycline hydrochloride (0.0276 min^{-1}), which is 4.78 times more than CN and 2.36 times more than tubular g-C_3N_4[128].

3.3.5 Compound modification

Various modification methods can effectively enhance the ability of photocatalysts to degrade organic pollutants in visible light, but there are still some difficulties to overcome. Therefore, more and more methods are needed to modify photocatalytic materials[13,108,129–158] (Table 6). For example, the research results show that nanomaterials can significantly improve the catalytic capacity compared with ordinary materials. Nanomaterials as catalysts have large specific surface area, contact area and useful active particle effect, which is the

Table 6 Summary of the results for compound modification photocatalyst systems

Photocatalyst and dosage		Organic pollutant and concentrations	Photodegradation efficiency	Ref.
TiO_2	NP-Fe_3O_4/GO-TiO_2 (80 mg)	[Rh B] = 20 mg·L^{-1}	180 min, over 85%	[129]
	N-TiO_2 @SiO_2@Fe_3O_4 (50 mg)	[PPCPs] = 2 mg·L^{-1}	5 h, 94% (IBU) 5 h, 93% (BZP-3) 9 h, 71%(CBZ) 9 h, 71% (CBZ)	[130]
	Fe_3O_4@SiO_2@TiO_2-Co/rGO (0.3 g)	[MB] = 10 mg·L^{-1}	160 min, 98.9%	[131]
	S-N/$CoFe_2O_4$@rGO@TiO_2 (80 mg)	[Organic dyes] = 5 mg·L^{-1}	120 min, 100% (MO) 90% (MB); 65% (Rh B)	[132]
	S-Bi-F-TiO_2/SiO_2 (500 mg)	[Acrylonitrile] = 10 mg·L^{-1}	6 min, 81.9%	[133]
	CeO_x@C-TiO_2 (50 mg)	[TC] = 40 mg·L^{-1}	180 min, 83.5%	[134]
	Black anatase-TiO_2 (20 mg)	[TC] = 10 mg·L^{-1}	270 min, 66.2%	[108]

(Continued)

Photocatalyst and dosage		Organic pollutant and concentrations	Photodegradation efficiency	Ref.
ZnO	ZnO/N-rGO (100 mg)	[2,4-DCP] = 10 mg·L^{-1}	60 min, over 50%	[135]
	ZnO/Fe_3O_4/g-C_3N_4 (10 mg)	[Azo dyes] = 30 mg·L^{-1}	150 min, 97.9% (MO); 98.1% (AYR); 83.4% (OG)	[136]
	ZnO/GO/Ag_3PO_4 (50 mg)	[TC] = 30 mg·L^{-1}	75 min, 96.3%	[137]
	Ag_3PO_4/g-C_3N_4/ZnO (30 mg)	[TC] = 30 mg·L^{-1}	180 min, 90.0% (Sunlight) 88.5% (Vis-Light)	[138]
	Fe_3O_4/ZnO/Si_3N_4 (20 mg)	[MO and SY] = 50 mg·L^{-1}	90 min, 96% (MO) 90 min, 90% (SY)	[13]
	La-ZnO/SiO_2 (15 mg)	[MG] = 15 mg·L^{-1}	140 min, 96.1% (MG)	[139]
	ZnO/CdS/GO (50 mg)	[MO] = 20 mg·L^{-1}	120 min, 100%	[140]
	AC@Au/ZnO (6 mg)	[Gemifloxacin] = 20 mg·L^{-1}	35 min, 98.0%	[141]
	$MnFe_2O_4$/ZnO/CQDs (62.5 mg)	[Gentamicin] = 50 mg·L^{-1}	120 min, 69.1%	[142]
	Ce/ZnO/Al_2O_3 (23 g)	[AR88 azo dye] = 20 mg·L^{-1}	240min, over 95%	[143]
	Fe-ZnO/WO_3 (100 mg)	[LVF] = 10 mg·L^{-1}	180 min, 96%	[144]
	ZnO/Zn_2TiO_4/GO (0.88 g·L^{-1})	[CEF] = 10 mg·L^{-1}	115 min, 71.4%	[145]
g-C_3N_4	S-CQDs/g-C_3N_4 (1 g·L^{-1})	[TC] = 20 mg·L^{-1}	40 min, 82.7%	[146]
	g-C_3N_4/PDI@NH_2-MIL-53(Fe) (10 mg)	[Organic pollutants] = 50 mg·L^{-1}	60 min, 90% (TC) 150 min, 78% (CBZ) 10 min, 100% (BPA) 30 min, 100% (PNP)	[147]
	g-C_3N_4/PDI@NH_2-MIL-53(Fe) (10 mg)	[Organic pollutants] = 50 mg·L^{-1}	60 min, 90% (TC) 150 min, 78% (CBZ) 10 min, 100% (BPA) 30 min, 100% (PNP)	[147]
	Ag/g-C_3N_4 /Bi_3TaO_7 (25 mg)	[SMZ] = 20 mg·L^{-1} [MO] = 5 mg·L^{-1}	25 min, 98% (SMZ) 40 min, 89% (MO)	[148]
	Ag_3PO_4/$Co_3(PO_4)_2$/g-C_3N_4 (50 mg)	[TC] = 10 mg·L^{-1}	120 min, 88%	[149]
	Bi_2MoO_6/g-C_3N_4/Au (5 mg)	[Rh B] = 5 mg·L^{-1}	40 min, 97.6%	[150]
	Cu_3P-$ZnSnO_3$/g-C_3N_4 (50 mg)	[TC] = 10 mg·L^{-1}	60 min, 98.45%	[151]
	Ag-AgCl/WO_3/g-C_3N_4 (50 mg)	[TMP] = 4 mg·L^{-1}	30 min, 99.9%	[152]
	CDs/g-C_3N_4/SnO_2 (10 mg)	[IDM] = 10 mg·L^{-1}	80 min, 90.8%	[153]
	Ag-g-C_3N_4/SnS_2 (20 mg)	[TC] = 15 mg·L^{-1}	150 min, 94.9%	[154]
	N/$K_4Nb_6O_{17}$/g-C_3N_4 (100 mg)	[Rh B] = 1 mg·L^{-1}	60 min, 100%	[155]
	FeOOH NPs/Nvac-CNNS (g-C_3N_4) (40 mg)	[OTC] = 10 mg·L^{-1}	90 min, 92.8%	[156]
	Ag_3PO_4/g-C_3N_4@MoS_2 (30 mg)	[AMA] = 20 mg·L^{-1}	90 min, 100%	[157]
	TiO_2@g-C_3N_4@BC (200 mg)	[CIP] = 20 mg·L^{-1}	60 min, 89.2%	[158]

most outstanding characteristic. However, with the decrease in particle size, nanoparticle catalysts are not easy to disperse and difficult to recover, so it is a good solution to this problem to load the catalytic material with porous materials mainly composed of magnetic materials. Qi et al.[129] prepared a novel magnetic GO-TiO_2 composite (Fe_3O_4/GO-TMC), which has a removal efficiency for Rh B over 85% under visible light irradiation within 180 min. Meanwhile, for the as-synthesized Fe_3O_4/GO-TMC no obvious decline in degradation efficiency was observed after at least five cycles and it was easier to recycle due to magnetic material doping. In addition, there have several other magnetically supported composite photocatalysts

have been used for the degradation of pharmaceuticals and personal care products[130], dyes[131,132,136] and antibiotics[142] with useful effects.

In addition to being easy to recycle, ternary heterojunctions provide better photocatalytic performance than standard catalysts. GO is a new type of carbon material with a two-dimensional honeycomb lattice structure, which has excellent mechanical, thermal and electrical properties. GOs can be combined with others photocatalytic materials to achieve synergistic treatment of wastewater pollutants[135,137,140,145]. The research results revealed that the ZnO/GO/Ag_3PO_4 composite provides higher photocatalytic activity for TC degradation under visible light than pure Ag_3PO_4, and ZnO/GO/Ag_3PO_4, with 96.3% degradation efficiency of TC within 75 min. Compared to Ag_3PO_4, which lost significant photocatalytic efficiency after three cycles of use, ZnO/GO/Ag_3PO_4 maintained relatively high photocatalytic performance after three cycles, indicating the stability of the photocatalyst. Through GO, the photogenerated electrons can rapidly transfer from Ag_3PO_4 to ZnO, so efficiently avoid the reduction of Ag^+[137].

Biochar is a solid substance rich in carbon produced by the pyrolysis of biomass under the condition of oxygen isolation. It has a large specific surface area and diverse functional groups, offering excellent adsorption, electrical conductivity and chemical stability, making it widely used as a carrier. In addition, the excellent electrical conductivity of biochar contributes to the transfer of photogenerated electrons, which can effectively reduce the compounding rate of photogenerated electrons and holes on the photocatalysts surface, and thus improve the photocatalytic efficiency. Faisal et al.[141] produce the ZnO doped by activated carbon (AC) and Au nanoparticles by the hydrothermal and ultrasonication methods. The high-efficiency AC@Au/ZnO framework provided impressive results with 98.0% destruction of the gemifloxacin mesylate drug, being 2.21 times higher than pure ZnO and 1.63 times than Au/ZnO. Wang et al.[158] loaded TiO_2/g-C_3N_4 with bamboo biochar and used it to degrade the ciprofloxacin under visible light giving 89.2% with 60 min. This material also had suitable stability and high photocatalytic activity even after five cycles.

Loading hard to recover and easily aggregating photocatalyst materials onto a loose, porous carriers with a large specific surface area can improve catalyst recovery, enhance photocatalyst diversity and utilization rate, and boost photocatalytic efficiency.

4 Cost-effectiveness of photocatalysts preparation

Photocatalytic oxidation technology has broad application prospects in the fields of energy production, pollution treatment, and environmental protection. It is an economical, environmentally-friendly and sustainable way to degrade organic pollutants in wastewater through photocatalytic degradation. However, to promote their wider application, not only does photocatalytic efficiency need to be enhanced through various modification methods, but also the cost of synthetic materials needs to be acceptable. For example, the deposition of Au, Ag, Pd and other noble metals on photocatalytic materials increased the absorption capacity of the catalyst system to visible light[96–100] but the cost was too high. As shown in Table 7, several photocatalysts were selected, and the cost of photocatalytic materials synthesized by different methods is analyzed based on the market raw material prices and civil electricity charges (0.6 yuan·kWh^{-1} of electricity) in China.

Through the comparison of several modification methods, it can be concluded that in the preparation process of photocatalytic materials, the high-cost is partly due to electricity costs when using ovens, muffle furnaces and tube furnaces[89,104,120,126,158], but also the cost of materials[99–101,103,128–137]. In addition, the method used to synthesize materials is also a major factor in the cost. Given that the sol-gel method to synthesize photocatalytic materials at lower temperatures, the consumption of electric energy is less, but the raw materials used in sol-gel are expensive[158–163]. Compared to sol-gel methods, hydrothermal synthesis uses cheaper, easily obtained raw materials, but its high-temperature, high-pressure steps increase equipment dependence and constrain its development[164–168]. In addition, as found in two studies[169,170], the modification of photocatalytic materials can also be achieved by using functional components in solid waste. This approach simultaneously reduces raw material expenses and achieves waste utilization. Further evaluation of simpler, low-energy synthesis methods is essential for effectively reducing the deployment costs of photocatalytic oxidation processes. Simple synthesis methods offer several key advantages. In terms of ease of implementation, they typically involve fewer steps and require less specialized equipment, making them more accessible to researchers and industries with limited resources. Additionally, simple methods are more user-friendly and can

Table 7 Materials and manufacturing cost of photocatalyst synthesis

Photocatalyst		Cost (yuan)	Ref.
TiO_2	Cu/TiO_2 (30 mg)	4.72	[82]
	N/TiO_2 (50 mg)	1.83	[89]
	Ag/TiO_2 (25 mg)	1.27	[97]
	$SnIn_4S_8$/TiO_2 (20 mg)	22.76	[109]
	D35 Dye-sensitized/TiO_2 (8 mg)	11.30	[124]
	Chl Dye-sensitized/TiO_2 (250 mg)	13.01	[125]
	CQDs/TiO_2 (4 mg)	18.71	[126]
	NP-Fe_3O_4/GO-TiO_2 (80 mg)	19.34	[129]
ZnO	Fe^{3+}/ZnO (800 mg)	17.34	[85]
	N/ZnO (10 mg)	2.74	[91]
	Ag/ZnO (1 g)	19.30	[98]
	Nd-V-ZnO (180 mg)	14.67	[100]
	Au/Pd/ZnO (0.5 mg)	23.56	[101]
	$NaBiS_2$/ZnO (10 mg)	11.88	[112]
	AC@Au/ZnO (6 mg)	8.16	[141]
g-C_3N_4	N/g-C_3N_4 (50 mg)	7.87	[95]
	Au/g-C_3N_4 (1 g)	18.15	[99]
	CoP/g-C_3N_4 (40 mg)	17.43	[121]
	BPQDs/g-C_3N_4 (30 mg)	21.10	[128]
	ZnO/GO/Ag_3PO_4 (50 mg)	21.22	[137]
	TiO_2@g-C_3N_4@BC (200 mg)	14.32	[158]

be performed without extensive training or highly specialized facilities. For energy efficiency, low-energy synthesis can be achieved by using lower temperatures, shorter reaction times or avoiding energy-intensive steps, such as high-temperature calcination or high-pressure processes. By combining these benefits, simpler and low-energy synthesis methods can significantly lower costs while maintaining effectiveness, making them an attractive option for the widespread adoption of photocatalytic oxidation technologies. Therefore, a comprehensive assessment of raw material costs, energy consumption, waste generation and potential environmental risks is required. Life cycle assessment is helpful for a comprehensive understanding of the environmental impact during the synthesis and use of photocatalytic materials[171]. This assessment is a systematic approach for assessing the environmental impact of a product or process throughout its entire life cycle, from raw material extraction to final disposal. For example, the preparation of some metal oxide photocatalysts may require calcination at high temperatures, which consumes a significant amount of energy. By applying life cycle assessment, it is possible to quantify the energy inputs at each stage of the life cycle of the material, from raw material extraction to final product formation.

There are still many problems needing further research for the development of suitable methods for photocatalytic material synthesis. For example, many researches are doing imitative or repetitive work, and do not give attention to innovation of basic theory. Therefore, there is a need to strengthen pioneering and innovative research on basic theories and focus on innovative synthesis methods, such as the use of cheap and readily available materials to synthesize new photocatalytic materials at room temperature.

5 Conclusions and outlooks

Photocatalytic oxidation process has good application prospect

in degrading organic pollutants in wastewater. However, it is still in the experimental stage due to some problems. To apply photocatalytic oxidation technology to the treatment of wastewater from livestock production, the following five key challenges should be prioritized in photocatalytic material modifications and process optimization,

Enhancing visible light utilization. There is a need to expand the visible light response range of photocatalysts and develop new materials. Doping and loading methods can improve photocatalytic materials, but the visible light utilization rate is still low, with limited actual application value. Further research needs to improve visible light utilization ratio.

Sustainable synthesis methods. Compound photocatalysts have complicated synthesis process due to various raw materials and strict reaction conditions like high temperature and pressure. Attention should be given to simplicity, low energy consumption and high efficiency in new material synthesis.

Reducing cost of raw materials. Photocatalysts with noble metal elements increase raw material cost. When developing such materials, improving noble metal utilization rate and adopting convenient synthesis methods are important. Also, low-cost alternatives to noble metals should be considered more, as continuing to develop high-cost noble metal photocatalysts has limited practical value.

Evaluating photocatalysts in practical applications. Evaluating the efficiency of photocatalytic materials using real wastewater and natural sunlight is of practical significance. Current studies often rely on single specific pollutants and simulated light sources, but real wastewater is complex. The presence of multiple pollutants, electrolytes, organic substances and inhibitors (e.g., ammonia and nitrites) in wastewater can reduce photocatalytic efficiency by scavenging radicals, blocking light and competing for active sites. Additionally, natural sunlight is more unstable than simulated light sources, with varying intensity influenced by weather, season and location, which can slow pollutant degradation efficiency.

Exploring photocatalytic reaction mechanisms. The degradation pathways of intermediates and pollutants vary due to the complexity of photocatalytic mechanism, different catalytic materials and environmental factors. Evaluating the intermediates of photocatalytic reactions is necessary. Raman spectroscopy, HRMS, TOF-MS and DFT calculations and other techniques can be used to study the electronic structure of photocatalysts, predict the energy levels of reactants, intermediates and products as well as the activation energy of reactions, and investigate dynamic processes, such as lattice vibration and hydrogen adsorption in reactions. It is important to be aware that some organic photocatalysts may produce toxic byproducts during degradation processes. Conducting thorough toxicity assessments and ensuring that the materials meet safety standards is essential.

Developing new materials to enhance visible light utilization often involves complex synthesis processes and increased costs, which can constrain scalability and practical application. Meanwhile, the use of noble metals raises material costs, further emphasizing the need for low-cost alternatives and simpler synthesis methods. Understanding the photocatalytic reaction mechanism and intermediate products is crucial for designing better materials with optimized properties, such as improved visible light absorption and charge separation efficiency. However, synthesis complexity material and cost can limit the feasibility of implementing these advanced materials in real-world applications, such as treating actual wastewater with natural sunlight.

Addressing these interconnected challenges requires a balanced strategy that focuses on enhancing visible light utilization, simplifying synthesis processes, reducing costs, and evaluating materials under real-world conditions. This holistic approach is essential for advancing sustainable and practical photocatalyst technologies, ultimately driving their broader application in wastewater treatment. In the short term, the development of photocatalytic materials still needs to focus on enhancing the utilization of visible light and simplifying the synthesis process, so as to promote the application of photocatalytic oxidation technology in actual production. On this basis, further examination of the synthesis and reaction mechanisms of photocatalytic materials to enhance theoretical knowledge reserves. In the long term, the goal is to develop photocatalytic materials and processes that are not only highly efficient but also sustainable and cost-effective. This includes finding low-cost, abundant raw materials and developing energy-efficient synthesis methods that can be easily scaled up for industrial applications.

Acknowledgements

This work was supported by National Natural Science Foundation of China (22209099); Shanxi Agricultural University high-level talent research project, China (2022XG18); Natural Science Foundation of Shanxi Province, China (202103021224130); Natural Science Foundation of Shandong Province, China (ZR2021ME202); Shanxi Postgraduate Education Innovation Project, China (2022Y316).

Compliance with ethics guidelines

Bo Sun, Xiaona Pan, Xingxing Qiao, Wenlong Bi, Yichen Hao, Junmei Qin, Qingjie Hou, and Fenwu Liu declare that they have no conflicts of interest or financial conflicts to disclose. This article does not contain any studies with human or animal subjects performed by any of the authors.

REFERENCES

1. Robles-Jimenez L E, Aranda-Aguirre E, Castelan-Ortega O A, Shettino-Bermudez B S, Ortiz-Salinas R, Miranda M, Li X, Angeles-Hernandez J C, Vargas-Bello-Pérez E, Gonzalez-Ronquillo M. Worldwide traceability of antibiotic residues from livestock in wastewater and soil: a systematic review. *Animals*, 2021, **12**(1): 60
2. Hayder G, Naim R M. Biochar-based nanocomposites from waste biomass: a sustainable approach for wastewater treatment and renewable bioenergy. *Frontiers of Agricultural Science and Engineering*, 2025, **12**(1): 117–147
3. Wang H, Xu J, Liu X, Sheng L, Zhang D, Li L, Wang A. Study on the pollution status and control measures for the livestock and poultry breeding industry in northeastern China. *Environmental Science and Pollution Research International*, 2018, **25**(5): 4435–4445
4. Wang R, Wang Q, Dong L, Zhang J. Cleaner agricultural production in drinking-water source areas for the control of non-point source pollution in China. *Journal of Environmental Management*, 2021, **285**: 112096
5. Serwecińska L. Antimicrobials and antibiotic-resistant bacteria: a risk to the environment and to public health. *Water*, 2020, **12**(12): 3313
6. Liu L, Xin Y, Huang X, Liu C. Response of antibiotic resistance genes in constructed wetlands during treatment of livestock wastewater with different exogenous inducers: antibiotic and antibiotic-resistant bacteria. *Bioresource Technology*, 2020, **314**: 123779
7. Wang M, Zhang Q, Li Y, Bak M P, Feng S, Kroeze C, Meng F, Micella I, Strokal V, Ural-Janssen A, Strokal M. Water pollution and agriculture: multi-pollutant perspectives. *Frontiers of Agricultural Science and Engineering*, 2023, **10**(4): 639–647
8. Davies K R, Cherif Y, Pazhani G P, Anantharaj S, Azzi H, Terashima C, Fujishima A, Pitchaimuthu S. The upsurge of photocatalysts in antibiotic micropollutants treatment: materials design, recovery, toxicity and bioanalysis. *Journal of Photochemistry and Photobiology C, Photochemistry Reviews*, 2021, **48**: 100437
9. Loebsack G, Yeung K K C, Berruti F, Klinghoffer N B. Impact of biochar physical properties on adsorption mechanisms for removal of aromatic aqueous contaminants in water. *Biomass and Bioenergy*, 2025, **194**: 107617
10. Feng Y, Liu W, Mu C, Zhong L, He Z, Zhang L, Xue J. Highly effective Pb(II) adsorption using physical–chemical double crosslinked polyvinyl alcohol-coated nano-calcium carbonate aerogel beads. *Chemical Physics Letters*, 2025, **861**: 141832
11. Vancsik A, Szabó L, Bauer L, Pirger Z, Karlik M, Kondor A C, Jakab G, Szalai Z. Impact of land use-induced soil heterogeneity on the adsorption of fluoroquinolone antibiotics, tested on organic matter pools. *Journal of Hazardous Materials*, 2024, **474**: 134704
12. Kandar B, Ghorui N, Datta C, Ghanta K C, Dutta S. Treatment of biologically treated synthetic refinery wastewater using *Stenotrophomonas maltophilia* sp. NITD 24: experiment and analysis. *Journal of Environmental Chemical Engineering*, 2025, **13**(3): 116305
13. Gasana Z, Kayiranga A, Nizeyimana J C, Tian S, Rugema J, You L, Huang X, Su J Q. Removal of antibiotics and antibiotic resistance genes using microalgae-based wastewater treatment system: a bibliometric review and mechanism analysis. *Journal of Water Process Engineering*, 2025, **72**: 107496
14. Gubitosa J, Rizzi V, Fini P, Nuzzo S, Cosma P. The adsorption efficiency of regenerable chitosan-TiO_2 composite films in removing 2,4-dinitrophenol from water. *International Journal*

of Molecular Sciences, 2023, **24**(10): 8552

15. Masula K, Bhongiri Y, Raghav Rao G, Vijay Kumar P, Pola S, Basude M. Evolution of photocatalytic activity of CeO_2–Bi_2O_3 composite material for wastewater degradation under visible-light irradiation. *Optical Materials*, 2022, **126**: 112201
16. Vaishnav S, Saini T, Chauhan A, Gaur G K, Tiwari R, Dutt T, Tarafdar A. Livestock and poultry farm wastewater treatment and its valorization for generating value-added products: recent updates and way forward. *Bioresource Technology*, 2023, **382**: 129170
17. Chen K, Scott J, Qu F, Dong W, Tsang D C W, Li W. Advanced cement-based photocatalytic materials: strategies for agglomeration control, aging resistance and process optimisation. *Journal of Building Engineering*, 2025, **112**: 113816
18. Carey J H, Lawrence J, Tosine H M. Photodechlorination of PCB's in the presence of titanium dioxide in aqueous suspensions. *Bulletin of Environmental Contamination and Toxicology*, 1976, **16**(6): 697–701
19. Gade R, Ahemed J, Yanapu K L, Abate S Y, Tao Y T, Pola S. Photodegradation of organic dyes and industrial wastewater in the presence of layer-type perovskite materials under visible light irradiation. *Journal of Environmental Chemical Engineering*, 2018, **6**(4): 4504–4513
20. Gade R, Basude M, Simhachalam N B, v R D, Pola S, Chetti P. Synthesis of titanates for photomineralization of industrial wastewater and organic pollutants. *Environmental Science. Water Research & Technology*, 2022, **8**(12): 3065–3078
21. Venkateshwar Rao D, Subburu M, Gade R, Basude M, Chetti P, Simhachalam N B, Nagababu P, Bhongiri Y, Pola S. A new Zn(ii) complex-composite material: piezo-enhanced photomineralization of organic pollutants and wastewater from the lubricant industry. *Environmental Science. Water Research & Technology*, 2021, **7**(10): 1737–1747
22. Xu W Q, Wang Y X, He H, Yang J, Yang Y, Ma J Z, Li C Q, Zhu T Y. Insight into hydroxyl groups in anchoring Ir single–atoms on vacancy–deficient rutile TiO_2 supports for selective catalytic oxidation of ammonia. *Applied Catalysis B. Applied Catalysis B: Environmental*, 2024, **345**: 123684
23. Parikirala R, Kore R, Rohini V, Venkateshwar Rao D V, Chetti P, Pola S. Synthesis of new Cu/Zn (II) complexes for sonophotocatalysis for mineralization of pesticides and agrochemical wastewater. *Journal of Environmental Chemical Engineering*, 2024, **12**(5): 113471
24. Vallavoju R, Kore R, Radhika P, Subburu M, Gade R, Basude M, Pola S, Chetti P. Enhanced piezo-photocatalytic properties of new salophen based Ti (IV) complexes. *Inorganic Chemistry Communications*, 2023, **148**: 110272
25. Masula K, Sreedhar P V, Vijay Kumar P, Bhongiri Y, Pola S, Basude M. Synthesis and characterization of NiO–Bi_2O_3 nanocomposite material for effective photodegradation of the dyes and agricultural soil pollutants. *Materials Science in Semiconductor Processing*, 2023, **160**: 107432
26. Xu B T, Ahmed M B, Zhou J L, Altaee A. Visible and UV photocatalysis of aqueous perfluorooctanoic acid by TiO_2 and peroxymonosulfate: process kinetics and mechanistic insights. *Chemosphere*, 2020, **243**: 125366
27. Mancuso A, Sacco O, Vaiano V, Sannino D, Pragliola S, Venditto V, Morante N. Visible light active Fe-Pr Co-doped TiO_2 for water pollutants degradation. *Catalysis Today*, 2021, **380**: 93–104
28. Yu X H, Yu L, Wang H T, Duan Y, Li X F, Zhao X, Wei H Z. Upcycling waste biomass to biochar: feedstocks, catalytic mechanisms, and applications in advanced oxidation for wastewater decontamination. *Langmuir*, 2025, **41**(1): 6–26
29. Khalid A, Ahmad P, Almukhlifi H A, Aldosari H H, Hossin M M, Ahmed A, Timoumi A, Alomayri T. Construction of highly efficient titanium dioxide adorned with graphitic carbon nitride with improved visible light-harvesting ability for the photocatalytic degradation of organic dyes. *Inorganic Chemistry Communications*, 2025, **176**: 114204
30. Pham M N, Nishimura F, Lan J C W, Khoo K S. Recent advancement of eliminating antibiotic resistance bacteria and antibiotic resistance genes in livestock waste: a review. *Environmental Technology & Innovation*, 2024, **36**: 103751
31. Li H K, Shen M C, Li M Y, Tao S Y, Li T H, Yang Z X. Removal of microplastics and resistance genes in livestock and aquaculture wastewater: current knowledge and future directions. *Journal of Environmental Chemical Engineering*, 2024, **12**(5): 113384
32. Ayinde W B, Ikumi D, Basitere M. Veterinary antibiotic removal from poultry slaughterhouse (PSH) wastewater: a mini-review of environmental nanoremediation techniques. *Environmental Technology Reviews*, 2025, **14**(1): 359–370
33. Gao R, Ding S J, Liu Z Z, Jiang H M, Liu G, Fang J. Recent advances and perspectives of biochar for livestock wastewater: modification methods, applications, and resource recovery. *Journal of Environmental Chemical Engineering*, 2024, **12**(5): 113678
34. Babu Ponnusami A, Sinha S, Ashokan H, V Paul M, Hariharan S P, Arun J, Gopinath K P, Hoang Le Q, Pugazhendhi A. Advanced oxidation process (AOP) combined biological process for wastewater treatment: a review on advancements, feasibility and practicability of combined techniques. *Environmental Research*, 2023, **237**: 116944
35. Huang S S, Wang G D, Liu J Q, Du C F, Su Y G. A novel $CuBi_2O_4$/BiOBr direct Z-scheme photocatalyst for efficient antibiotics removal: synergy of adsorption and photocatalysis on degradation kinetics and mechanism insight. *ChemCatChem*, 2020, **12**(17): 4431–4445
36. Ma L Z, Duan J L, Ji B, Liu Y F, Li C J, Li C, Zhao W F, Yang

Z. Ligand-metal charge transfer mechanism enhances TiO_2/Bi_2WO_6/rGO nanomaterials photocatalytic efficient degradation of norfloxacin under visible light. *Journal of Alloys and Compounds*, 2021, **869**: 158679

37. He J Z, Zhang Y Z, Guo Y, Rhodes G, Yeom J, Li H, Zhang W. Photocatalytic degradation of cephalexin by ZnO nanowires under simulated sunlight: kinetics, influencing factors, and mechanisms. *Environment International*, 2019, **132**: 105105
38. Govarthanan M, Mythili R, Kim W, Alfarraj S, Ali Alharbi S. Facile fabrication of (2D/2D) MoS_2@MIL-88(Fe) interface-driven catalyst for efficient degradation of organic pollutants under visible light irradiation. *Journal of Hazardous Materials*, 2021, **414**: 125522
39. Clarizia L, Vitiello G, Bericat Vadell R, Sá J, Marotta R, Di Somma I, Andreozzi R, Luciani G. Effect of synthesis method on reaction mechanism for hydrogen evolution over Cu_xO_y/TiO_2 photocatalysts: a kinetic analysis. *International Journal of Molecular Sciences*, 2023, **24**(3): 2004
40. Ukarde T M, Pawar H S. A Cu doped TiO_2 catalyst mediated Catalytic Thermo Liquefaction (CTL) of polyolefinic plastic waste into hydrocarbon oil. *Fuel*, 2021, **285**: 119155
41. Yasuda M, Matsumoto T, Yamashita T. Sacrificial hydrogen production over TiO_2-based photocatalysts: polyols, carboxylic acids, and saccharides. *Renewable & Sustainable Energy Reviews*, 2018, **81**: 1627–1635
42. Zhao X, Liu Q X, Li Q, Yin Y H, Zheng M, Luo F Q, Gu H Q, Jiang B. Sea urchin-like covalent organic frameworks/TiO_2 heterostructure for enhanced photocatalytic CO_2 conversion. *Journal of Colloid and Interface Science*, 2025, **685**: 1068–1076
43. Babu S G, Karthik P, John M C, Lakhera S K, Ashokkumar M, Khim J, Neppolian B. Synergistic effect of sono-photocatalytic process for the degradation of organic pollutants using CuO-TiO_2/rGO. *Ultrasonics Sonochemistry*, 2019, **50**: 218–223
44. Ling L L, Feng Y W, Li H, Chen Y, Wen J Y, Zhu J, Bian Z F. Microwave induced surface enhanced pollutant adsorption and photocatalytic degradation on Ag/TiO_2. *Applied Surface Science*, 2019, **483**: 772–778
45. Wan X J, Ke H Q, Yang G H, Tang J N. Carboxyl-modified hierarchical wrinkled mesoporous silica supported TiO_2 nanocomposite particles with excellent photocatalytic performances. *Progress in Natural Science*, 2018, **28**(6): 683–688
46. Navidpour A H, Xu B T, Ahmed M B, Zhou J L. Immobilization of TiO_2 and ZnO by facile surface engineering methods to improve semiconductor performance in photocatalytic wastewater treatment: a review. *Materials Science in Semiconductor Processing*, 2024, **179**: 108518
47. Kanakaraju D, anak Kutiang F D, Lim Y C, Goh P S. Recent progress of Ag/TiO_2 photocatalyst for wastewater treatment: doping, co-doping, and green materials functionalization. *Applied Materials Today*, 2022, **27**: 101500
48. Ghaderi A, Sadr M H, Gharagozlou M, Sadjadi S. Improvement of photocatalytic activity of TiO_2 via a dual approach, consisting of iron doping and incorporation in Cu-based metal-organic framework. *Journal of the Indian Chemical Society*, 2025, **102**(4): 101636
49. Han B Q, Wang C S, Yang W Y, Hu G Q, Zhang X Y, Wang B B, Wang H R. Hydrothermal synthesis of spherical nanoflower ZnO with highly sensitive isoprene sensing performance. *Journal of Alloys and Compounds*, 2025, **1023**: 180176
50. Wang Y, Xu S, Zhang H Y, Wang Y Y, Wang E M, He Z Y, Zhu J H, Lu X H, Zhang L L, Bai Y, Zhao K F, Gao Q W, Zeng J R, Yi Z G, Ming T Z, Li W, Mu L W. Highly dispersed CuO_x decorated ZnO photocatalyst for low-concentration methane removal. *Journal of Environmental Chemical Engineering*, 2024, **12**(6): 114954
51. Rong P, Ren S, Yu Q. Fabrications and applications of ZnO nanomaterials in flexible functional devices—A review. *Critical Reviews in Analytical Chemistry*, 2019, **49**(4): 336–349
52. Al-Shami A, Sibari A, Mansouri Z, El Kassaoui M, El Kenz A, Benyoussef A, Loulidi M, Jouiad M, El Moutaouakil A, Mounkachi O. Photocatalytic properties of ZnO: Al/MAPbI3/Fe_2O_3 heterostructure: first-principles calculations. *International Journal of Molecular Sciences*, 2023, **24**(5): 4856
53. Chen S T, Song X S, Song X C, Zhang Y. Novel electrochemical synthesis of N-doped ZnO–rGO films for the photoelectrocatalytic degradation of antibiotics. *Optical Materials*, 2024, **157**: 116308
54. Nurtono T, Abdul Ajiz H, Widiyastuti W, Setyawan H. Behavior of tunable ZnO quantum dots (QDs) stabilized by surfactant-free silica nanofluids in their visible luminescence spectra. *Advanced Powder Technology*, 2024, **35**(12): 104697
55. Raha S, Ahmaruzzaman M. ZnO nanostructured materials and their potential applications: progress, challenges and perspectives. *Nanoscale Advances*, 2022, **4**(8): 1868–1925
56. Jourshabani M, Lee B K, Shariatinia Z. From traditional strategies to Z-scheme configuration in graphitic carbon nitride photocatalysts: recent progress and future challenges. *Applied Catalysis B: Environmental*, 2020, **276**: 119157
57. Hussain S, Wang Y J, Guo L J, He T. Theoretical insights into the mechanism of photocatalytic reduction of CO_2 over semiconductor catalysts. *Journal of Photochemistry and Photobiology C, Photochemistry Reviews*, 2022, **52**: 100538
58. Zhao Y, Yang D Y, Yu C L, Yan H. A review on photocatalytic CO_2 reduction of g-C_3N_4 and g-C_3N_4-based photocatalysts modified by CQDs. *Journal of Environmental Chemical Engineering*, 2025, **13**(2): 115348
59. Tamilselvan R, Immanuel Selwynraj A. Enhancing biogas production through photocatalytic pretreatment of rice straw co-digested with cow dung and food waste using a novel g-

C_3N_4/SiO_2/bentonite catalyst. *Process Safety and Environmental Protection*, 2024, **187**: 799–809

60. Wang Y, Tan G Q, Dang M Y, Dong S H, Liu Y, Liu T, Ren H J, Xia A, Lv L. Study on surface modification of g-C_3N_4 photocatalyst. *Journal of Alloys and Compounds*, 2022, **908**: 164507
61. Jacob K A, Peter P M, Jose P E, Balakrishnan C J, Thomas V J. A simple method for the synthesis of anatase-rutile mixed phase TiO_2 using a convenient precursor and higher visible-light photocatalytic activity of Co–doped TiO_2. *Materials Today: Proceedings*, 2022, **49**: 1408–1417
62. Ding L, Yang S R, Liang Z Q, Qian X, Chen X Y, Cui H Z, Tian J. TiO_2 nanobelts with anatase/rutile heterophase junctions for highly efficient photocatalytic overall water splitting. *Journal of Colloid and Interface Science*, 2020, **567**: 181–189
63. He J, Du Y E, Bai Y, An J, Cai X M, Chen Y Q, Wang P F, Yang X J, Feng Q. Facile formation of anatase/rutile TiO_2 nanocomposites with enhanced photocatalytic activity. *Molecules*, 2019, **24**(16): 2996
64. Kovács Z, Molnár C, Gyulavári T, Magyari K, Tóth Z R, Baia L, Pap Z, Hernádi K. Solvothermal synthesis of ZnO spheres: tuning the structure and morphology from nano- to micro-meter range and its impact on their photocatalytic activity. *Catalysis Today*, 2022, **397–399**: 16–27
65. Goktas A, Modanlı S, Tumbul A, Kilic A. Facile synthesis and characterization of ZnO, ZnO: Co, and ZnO/ZnO: Co nano rod-like homojunction thin films: role of crystallite/grain size and microstrain in photocatalytic performance. *Journal of Alloys and Compounds*, 2022, **893**: 162334
66. Tian G Y, Xiang R Y, Chen B, Shi Z D, Huang W S, Han G F. "Branch-Flower buds" like palygorskite/ultra-small NiCu alloy composites for highly efficient catalytic reduction of 4-nitrophenol. *Applied Surface Science*, 2025, **689**: 162488
67. Chen Y Y, Gong W Y, Niu K, Wang X, Lin Y D, Lin D F, Jin H J, Luo Y J, Qian Q R, Chen Q H. Chitosan–NH_2 derived efficient Co_3O_4 catalyst for styrene catalytic oxidation: simultaneously regulating particle size and Co valence. *Journal of Colloid and Interface Science*, 2024, **659**: 439–448
68. Jin Z L, Xiao S J, Dong H R, Xiao J Y, Tian R, Chen J, Li Y J, Li L. Adsorption and catalytic degradation of organic contaminants by biochar: overlooked role of biochar's particle size. *Journal of Hazardous Materials*, 2022, **422**: 126928
69. Li Y F, Liu Z P. Particle size, shape and activity for photocatalysis on titania anatase nanoparticles in aqueous surroundings. *Journal of the American Chemical Society*, 2011, **133**(39): 15743–15752
70. Zhang B, He X, Ma X H, Chen Q H, Liu G C, Zhou Y M, Ma D, Cui C Y, Ma J, Xin Y J. *In situ* synthesis of ultrafine TiO_2 nanoparticles modified g-C_3N_4 heterojunction photocatalyst with enhanced photocatalytic activity. *Separation and Purification Technology*, 2020, **247**: 116932
71. Wang Y Q, Zhang M D, Zhao J M, Chen C, Zhou Y Y, Zheng X, Zhang C L. *In-situ* one-step synthesis of porous monolayer carbon nitride nanosheets doped with carbon quantum dots for photocatalytic degradation of Meloxicam. *Colloids and Surfaces. A, Physicochemical and Engineering Aspects*, 2022, **647**: 129042
72. Zhong J X, Jiang H, Wang Z L, Yu Z G, Wang L Z, Mueller J F, Guo J H. Efficient photocatalytic destruction of recalcitrant micropollutants using graphitic carbon nitride under simulated sunlight irradiation. *Environmental Science and Ecotechnology*, 2021, **5**: 100079
73. Muhmood T, Ahmad I, Haider Z, Haider S K, Shahzadi N, Aftab A, Ahmed S, Ahmad F. Graphene-like graphitic carbon nitride (g-C_3N_4) as a semiconductor photocatalyst: properties, classification, and defects engineering approaches. *Materials Today Sustainability*, 2024, **25**: 100633
74. Ding P R, Ji H D, Li P S, Liu Q M, Wu Y Y, Guo M, Zhou Z A, Gao S, Xu W L, Liu W, Wang Q, Chen S. Visible-light degradation of antibiotics catalyzed by titania/zirconia/graphitic carbon nitride ternary nanocomposites: a combined experimental and theoretical study. *Applied Catalysis B: Environmental*, 2022, **300**: 120633
75. Teng M Y, Liu H X, Lin B S, Zhou X Z, Zhou W. Preparation and photocatalytic properties of anatase TiO_2 with hollow hexagonal frame structure. *Nanomaterials*, 2022, **12**(9): 1409
76. Sun S Y, Hu Y Y, Xu M S, Cheng F, Zhang H, Li Z K. Photo-Fenton degradation of carbamazepine and ibuprofen by iron-based metal-organic framework under alkaline condition. *Journal of Hazardous Materials*, 2022, **424**: 127698
77. Xu T Z, Zheng H, Zhang P Y. Isolated Pt single atomic sites anchored on nanoporous TiO_2 film for highly efficient photocatalytic degradation of low concentration toluene. *Journal of Hazardous Materials*, 2020, **388**: 121746
78. Bhnar W, Bao A. Controlled synthesis of porous carbon materials from cow dung biomass and analysis of their adsorption properties: modulation of lignocellulosic fractions and pore structure formation. *Sustainable Materials and Technologies*, 2025, **44**: e01328
79. Guo X J, Song H Y, Du B R, Tan S W, Liu S B. Study on spectral selective manipulation characteristics of surface multilevel micro–nano structures by FDTD simulation. *International Journal of Molecular Sciences*, 2022, **23**(5): 2774
80. Lu F, Wang J G, Chang Z J, Zeng J. Uniform deposition of Ag nanoparticles on ZnO nanorod arrays grown on polyimide/Ag nanofibers by electrospinning, hydrothermal, and photoreduction processes. *Materials & Design*, 2019, **181**: 108069
81. Chen J J, Li Y Y, Cui T L, Shi Y, Wang R R, Liu X M, Liu G, Chen K K. Preparation and properties of g-C_3N_4 photocatalysts with hierarchical porous structure. *Chinese*

Journal of Inorganic Chemistry, 2020, **36**(5): 835–840 (in Chinese)

82. Qu X, Lin J B, Chaudhary J P, Sun B J, Wei F, Fan M M, Sun D P. Defect enrich ultrathin TiO_2 nanosheets for rapid adsorption and visible light mediated PPCPs degradation. *Chemosphere*, 2021, **268**: 128782
83. Zhang J, Yang C, Li S J, Xi Y X, Cai C L, Liu W G, Golosov D, Zavadski S, Melnikov S. Preparation of Fe^{3+} doped high-ordered TiO_2 nanotubes arrays with visible photocatalytic activities. *Nanomaterials*, 2020, **10**(11): 2107
84. Sheydaei M, Fattahi M, Ghalamchi L, Vatanpour V. Systematic comparison of sono-synthesized Ce-, La- and Ho-doped ZnO nanoparticles and using the optimum catalyst in a visible light assisted continuous sono-photocatalytic membrane reactor. *Ultrasonics Sonochemistry*, 2019, **56**: 361–371
85. Khan H, Habib M, Khan A, Boffito D C. A modified sol-gel synthesis to yield a stable Fe^{3+}/ZnO photocatalyst: degradation of water pollutants and mechanistic insights under UV and visible light. *Journal of Environmental Chemical Engineering*, 2020, **8**(5): 104282
86. Huong P T L, Van Quang N V, Tran M T, Trung D Q, Hop D T B, Tam T T H, Tu N, Dao V D. Excellent visible light photocatalytic degradation and mechanism insight of Co^{2+}-doped ZnO nanoparticles. *Applied Physics. A, Materials Science & Processing*, 2022, **128**(1): 24
87. Ou Q, Xu S X, Long Y L, Zhang X F. Porous visible light-responsive Fe^{3+}-doped carbon nitride for efficient degradation of sulfadiazine. *Environmental Science and Pollution Research International*, 2020, **27**(22): 27849–27858
88. Jiang L, Luo Z F, Li Y Z, Wang W, Li J J, Li J, Ao Y L, He J, Sharma V K, Wang J Q. Morphology- and phase-controlled synthesis of visible-light-activated S-doped TiO_2 with tunable S^{4+}/S^{6+} ratio. *Chemical Engineering Journal*, 2020, **402**: 125549
89. Huang J, Dou L, Li J Z, Zhong J B, Li M J, Wang T. Excellent visible light responsive photocatalytic behavior of N-doped TiO_2 toward decontamination of organic pollutants. *Journal of Hazardous Materials*, 2021, **403**: 123857
90. Alkorbi A S, Muhammad Asif Javed H, Hussain S, Latif S, Mahr M S, Mustafa M S, Alsaiari R, Alhemiary N A. Solar light-driven photocatalytic degradation of methyl blue by carbon-doped TiO_2 nanoparticles. *Optical Materials*, 2022, **127**: 112259
91. Tang C M, Chen C, Zhang H Y, Zhang J, Li Z J. Enhancement of degradation for nitrogen doped zinc oxide to degrade methylene blue. *Physica B, Condensed Matter*, 2020, **583**: 412029
92. Mirzaeifard Z, Shariatinia Z, Jourshabani M, Rezaei Darvishi S M. ZnO photocatalyst revisited: effective photocatalytic degradation of emerging contaminants using S-doped ZnO nanoparticles under visible light radiation. *Industrial & Engineering Chemistry Research*, 2020, **59**(36): 15894–15911
93. Guo F, Li M Y, Ren H J, Huang X L, Shu K K, Shi W L, Lu C Y. Facile bottom-up preparation of Cl-doped porous g-C_3N_4 nanosheets for enhanced photocatalytic degradation of tetracycline under visible light. *Separation and Purification Technology*, 2019, **228**: 115770
94. Jiang L B, Yuan X Z, Zeng G M, Liang J, Wu Z B, Yu H B, Mo D, Wang H, Xiao Z H, Zhou C. Nitrogen self-doped g-C_3N_4 nanosheets with tunable band structures for enhanced photocatalytic tetracycline degradation. *Journal of Colloid and Interface Science*, 2019, **536**: 17–29
95. Zhu D D, Zhou Q. X Nitrogen doped g-C_3N_4 with the extremely narrow band gap for excellent photocatalytic activities under visible light. *Applied Catalysis B: Environmental*, 2021, **281**: 119474
96. Guo W, Zou J H, Guo B B, Xiong J H, Liu C, Xie Z H, Wu L. Pd nanoclusters/TiO_2(B) nanosheets with surface defects toward rapid photocatalytic dehalogenation of polyhalogenated biphenyls under visible light. *Applied Catalysis B: Environmental*, 2020, **277**: 119255
97. Gang R Q, Xia Y, Xu L, Zhang L B, Ju S H, Wang Z, Koppala S. Size controlled Ag decorated TiO_2 plasmonic photocatalysts for tetracycline degradation under visible light. *Surfaces and Interfaces*, 2022, **31**: 102018
98. Podasca V E, Damaceanu M D. ZnO-Ag based polymer composites as photocatalysts for highly efficient visible-light degradation of Methyl Orange. *Journal of Photochemistry and Photobiology A Chemistry*, 2021, **406**: 113003
99. Alam U, Shah T A, Khan A, Muneer M. One-pot ultrasonic assisted sol-gel synthesis of spindle-like Nd and V codoped ZnO for efficient photocatalytic degradation of organic pollutants. *Separation and Purification Technology*, 2019, **212**: 427–437
100. Lee S J, Jung H J, Koutavarapu R, Lee S H, Arumugam M, Kim J H, Choi M Y. ZnO supported Au/Pd bimetallic nanocomposites for plasmon improved photocatalytic activity for methylene blue degradation under visible light irradiation. *Applied Surface Science*, 2019, **496**: 143665
101. Jiménez-Salcedo M, Monge M, Tena M T. An organometallic approach for the preparation of Au–TiO_2 and Au–g-C_3N_4 nanohybrids: improving the depletion of paracetamol under visible light. *Photochemical & Photobiological Sciences*, 2022, **21**(3): 337–347
102. Gao J Y, Zhu Y, Zeng L F, Liu X, Yang Y, Zhou Y Y. Recent advances on environmental behavior of Cu-based nanomaterials in soil-plant system: a review. *Journal of Environmental Management*, 2024, **361**: 121289
103. Jian F Y, Lu N, Zhao S J, Liang H T, Wei Z H, Liu A M, Tang H. Visible light degradation of organic pollutants using Cu modified TiO_2 supported on g-C_3N_4. *Journal of Alloys and Compounds*, 2025, **1014**: 178641

104. Ge Y J, Sun Q R, Bai H T, Li J D, Du X H. *In situ* production of hydrogen peroxide from Fe, Mo Co-doped N@TiO_2 for organic pollutant degradation. *Separation and Purification Technology*, 2025, **359**: 130644
105. Tian M, Ren X H, Ding S Y, Fu N, Wei Y J, Yang Z Y, Yao X Q. Effective degradation of phenol by activating PMS with bimetallic Mo and Ni Co-doped g-C_3N_4 composite catalyst: a Fenton-like degradation process promoted by non-free radical $^1O_2$. *Environmental Research*, 2024, **243**: 117848
106. Oskoei A, Khaleghi M, Sheibani S. Modification of MoS_2/ZnO nanocomposite for efficient photocatalytic degradation of water pollutants and hydrogen evolution. *Journal of Water Process Engineering*, 2025, **71**: 107404
107. Zhang M, Wang S, Li Z L, Liu C W, Miao R, He G, Zhao M, Xue J, Xia Z Y, Wang Y Q, Sun Z Q, Lv J G. Hydrothermal synthesis of MoS_2 nanosheet loaded TiO_2 nanoarrays for enhanced visible light photocatalytic applications. *RSC Advances*, 2019, **9**(6): 3479–3485
108. Wu S Q, Li X Y, Tian Y Q, Lin Y, Hu Y H. Excellent photocatalytic degradation of tetracycline over black anatase-TiO_2 under visible light. *Chemical Engineering Journal*, 2021, **406**: 126747
109. Wang J, Wang B Q, Zhang W L, Xiao Y, Xu H, Liu Y, Liu Z C, Zhang J M, Jiang Y H. Visible-light-driven double-shell $SnIn_4S_8$/TiO_2 heterostructure with enhanced photocatalytic activity for MO removal and Cr(VI) cleanup. *Applied Surface Science*, 2022, **587**: 152867
110. Zhu W, Xia Z, Shi B, Lü C. Water-triggered conversion of Cs_4PbBr_6@TiO_2 into Cs_4PbBr_6/$CsPbBr_3$@TiO_2 three-phase heterojunction for enhanced visible-light-driven photocatalytic degradation of organic pollutants. *Materials Today. Chemistry*, 2022, **24**: 100880
111. Mubarak M F, Selim H, Elshypany R. Hybrid magnetic core–shell TiO_2@$CoFe_3O_4$ composite towards visible light-driven photodegradation of Methylene blue dye and the heavy metal adsorption: isotherm and kinetic study. *Journal of Environmental Health Science & Engineering*, 2022, **20**(1): 265–280
112. Koutavarapu R, Lee G, Babu B, Yoo K, Shim J. Visible-light-driven photocatalytic activity of tiny ZnO nanosheets anchored on NaBiS2 nanoribbons *via* hydrothermal synthesis. *Journal of Materials Science Materials in Electronics*, 2019, **30**(11): 10900–10911
113. Jiang Z, Xiao C, Yin X Y, Xu L J, Liu C L, Wang H L. Facile preparation of a novel $Bi_{24}O_{31}Br_{10}$/nano-ZnO composite photocatalyst with enhanced visible light photocatalytic ability. *Ceramics International*, 2020, **46**(8): 10771–10778
114. Venugopal G, Thangavel S, Vasudevan V, Zoltán K. Efficient visible-light piezophototronic activity of ZnO-Ag_8S hybrid for degradation of organic dye molecule. *Journal of Physics and Chemistry of Solids*, 2020, **143**: 109473
115. Abdel-Aziz R, Ahmed M A, Abdel-Messih M F. A novel UV and visible light driven photocatalyst $AgIO_4$/ZnO nanoparticles with highly enhanced photocatalytic performance for removal of rhodamine B and indigo carmine dyes. *Journal of Photochemistry and Photobiology A Chemistry*, 2020, **389**: 112245
116. Manimozhi R, Mathankumar M, Gnana Prakash A P G. Synthesis of g-C_3N_4/ZnO heterostructure photocatalyst for enhanced visible degradation of organic dye. *Optik*, 2021, **229**: 165548
117. Guo F, Shi W L, Li M Y, Shi Y, Wen H B. 2D/2D Z-scheme heterojunction of $CuInS_2$/g-C_3N_4 for enhanced visible-light-driven photocatalytic activity towards the degradation of tetracycline. *Separation and Purification Technology*, 2019, **210**: 608–615
118. Feng Z, Zeng L, Zhang Q L, Ge S F, Zhao X Y, Lin H J, He Y M. *In situ* preparation of g-C_3N_4/$Bi_4O_5I_2$ complex and its elevated photoactivity in Methyl Orange degradation under visible light. *Journal of Environmental Sciences*, 2020, **87**: 149–162
119. Zhang Z Z, Pan Z W, Guo Y F, Wong P K, Zhou X J, Bai R B. *In-situ* growth of all-solid Z-scheme heterojunction photocatalyst of $Bi_7O_9I_3$/g-C_3N_4 and high efficient degradation of antibiotic under visible light. *Applied Catalysis B: Environmental*, 2020, **261**: 118212
120. Pan T, Chen D D, Xu W C, Fang J Z, Wu S X, Liu Z, Wu K, Fang Z Q. Anionic polyacrylamide-assisted construction of thin 2D–2D WO_3/g-C_3N_4 step-scheme heterojunction for enhanced tetracycline degradation under visible light irradiation. *Journal of Hazardous Materials*, 2020, **393**: 122366
121. Guo F, Huang X L, Chen Z H, Sun H R, Chen L Z. Prominent co-catalytic effect of CoP nanoparticles anchored on high-crystalline g-C_3N_4 nanosheets for enhanced visible-light photocatalytic degradation of tetracycline in wastewater. *Chemical Engineering Journal*, 2020, **395**: 125118
122. Oluwole A O, Olatunji O S. Photocatalytic degradation of tetracycline in aqueous systems under visible light irridiation using needle-like SnO_2 nanoparticles anchored on exfoliated g-C_3N_4. *Environmental Sciences Europe*, 2022, **34**(1): 5
123. Ismael M, Wark M. Photocatalytic activity of $CoFe_2O_4$/g-C_3N_4 nanocomposite toward degradation of different organic pollutants and their inactivity toward hydrogen production: the role of the conduction band position. *FlatChem*, 2022, **32**: 100337
124. Bai X, Yang L, Hagfeldt A, Johansson E M J, Jin P K. D35-TiO_2 nano-crystalline film as a high performance visible-light photocatalyst towards the degradation of *bis*-phenol A. *Chemical Engineering Journal*, 2019, **355**: 999–1010
125. Krishnan S, Shriwastav A. Application of TiO_2 nanoparticles sensitized with natural chlorophyll pigments as catalyst for visible light photocatalytic degradation of methylene blue.

Journal of Environmental Chemical Engineering, 2021, **9**(1): 104699

126. Shafique M, Mahr M S, Yaseen M, Bhatti H N. CQD/TiO_2 nanocomposite photocatalyst for efficient visible light-driven purification of wastewater containing methyl orange dye. *Materials Chemistry and Physics*, 2022, **278**: 125583
127. Liu W, Li Y Y, Liu F Y, Jiang W, Zhang D D, Liang J L. Visible-light-driven photocatalytic degradation of diclofenac by carbon quantum dots modified porous g-C_3N_4: mechanisms, degradation pathway and DFT calculation. *Water Research*, 2019, **151**: 8–19
128. Wang W J, Niu Q Y, Zeng G M, Zhang C, Huang D L, Shao B B, Zhou C Y, Yang Y, Liu Y X, Guo H, Xiong W P, Lei L, Liu S Y, Yi H, Chen S, Tang X. 1D porous tubular g-C_3N_4 capture black phosphorus quantum dots as 1D/0D metal-free photocatalysts for oxytetracycline hydrochloride degradation and hexavalent chromium reduction. *Applied Catalysis B: Environmental*, 2020, **273**: 119051
129. Qi H P, Wang H L, Zhao D Y, Wang X K. Synthesis of novel magnetic superstructure TiO_2 mesocrystal composites with enhanced visible-light photocatalytic activity. *Materials Research Bulletin*, 2019, **118**: 110516
130. Kumar A, Khan M, Fang L P, Lo I M C. Visible-light-driven N-TiO_2@SiO_2@Fe_3O_4 magnetic nanophotocatalysts: synthesis, characterization, and photocatalytic degradation of PPCPs. *Journal of Hazardous Materials*, 2019, **370**: 108–116
131. Fu C Z, Liu X, Wang Y, Li L, Zhang Z H. Preparation and characterization of Fe_3O_4@SiO_2@TiO_2–Co/rGO magnetic visible light photocatalyst for water treatment. *RSC Advances*, 2019, **9**(35): 20256–20265
132. Wei F Y, Wang H, Ran W, Liu T, Liu X T. Preparation of S–N Co-doped $CoFe_2O_4$@rGO@TiO_2 nanoparticles and their superior UV-Vis light photocatalytic activities. *RSC Advances*, 2019, **9**(11): 6152–6162
133. Li H L, Qiu L, Bharti B, Dai F W, Zhu M Y, Ouyang F, Lin L. Efficient photocatalytic degradation of acrylonitrile by Sulfur-Bismuth Co-doped F-TiO_2/SiO_2 nanopowder. *Chemosphere*, 2020, **249**: 126135
134. Yuan J Y, Pudukudy M, Hu T D, Liu Y, Luo X F, Zhi Y F, Su H F, Jiang L H, Shan S Y. CeO_x-coupled MIL-125-derived C-TiO_2 catalysts for the enhanced photocatalytic abatement of tetracycline under visible light irradiation. *Applied Surface Science*, 2021, **557**: 149829
135. Neena D, Kondamareddy K K, Humayun M, Mohan V B, Lu D Z, Fu D J, Gao W. Fabrication of ZnO/N-rGO composite as highly efficient visible-light photocatalyst for 2,4-DCP degradation and H_2 evolution. *Applied Surface Science*, 2019, **488**: 611–619
136. Wu Z S, Chen X Q, Liu X C, Yang X, Yang Y. A ternary magnetic recyclable ZnO/Fe_3O_4/g-C_3N_4 composite photocatalyst for efficient photodegradation of monoazo dye. *Nanoscale Research Letters*, 2019, **14**(1): 147
137. Zhu P F, Duan M, Wang R X, Xu J, Zou P, Jia H S. Facile synthesis of ZnO/GO/Ag_3PO_4 heterojunction photocatalyst with excellent photodegradation activity for tetracycline hydrochloride under visible light. *Colloids and Surfaces. A, Physicochemical and Engineering Aspects*, 2020, **602**: 125118
138. Zhu P F, Hu M, Duan M, Xie L S, Zhao M Y. High visible light response Z-scheme Ag_3PO_4/g-C_3N_4/ZnO composite photocatalyst for efficient degradation of tetracycline hydrochloride: preparation, properties and mechanism. *Journal of Alloys and Compounds*, 2020, **840**: 155714
139. Wang S, Chen Z K, Zhao Y, Sun C L, Li J Y. High photocatalytic activity over starfish-like La-doped ZnO/SiO_2 photocatalyst for malachite green degradation under visible light. *Journal of Rare Earths*, 2021, **39**(7): 772–780
140. Das D, Nandi P. Synthesis of CdS/GO modified ZnO heterostructure for visible light dye degradation applications. *Applied Surface Science*, 2021, **570**: 151260
141. Faisal M, Alsaiari M, Rashed M A, Harraz F A. Highly efficient biomass-derived carbon@Au/ZnO novel ternary photocatalyst for ultra-fast degradation of gemifloxacin drug. *Journal of Materials Research and Technology*, 2021, **14**: 954–967
142. Rahal M, Atassi Y, Alghoraibi I. Preparation of separable $MnFe_2O_4$/ZnO/CQDs as a visible light photocatalyst for Gentamicin treatment. *Materials Chemistry and Physics*, 2022, **286**: 126123
143. Kardeş M, Yılmaz H, Öztürk K. Pure and cerium-doped ZnO nanorods grown on reticulated Al_2O_3 substrate for photocatalytic degradation of Acid Red 88 azo dye. *Ceramics International*, 2022, **48**(5): 7093–7105
144. Tsai C K, Lee Y C, Nguyen T T, Horng J J. Levofloxacin degradation under visible-LED photo-catalyzing by a novel ternary Fe–ZnO/WO_3 nanocomposite. *Chemosphere*, 2022, **298**: 134285
145. Behineh E S, Solaimany Nazar A R S, Farhadian M, Moghadam M. Photocatalytic degradation of cefixime using visible light-driven Z-scheme ZnO nanorod/Zn_2TiO_4/GO heterostructure. *Journal of Environmental Management*, 2022, **316**: 115195
146. Wang W J, Zeng Z T, Zeng G M, Zhang C, Xiao R, Zhou C Y, Xiong W P, Yang Y, Lei L, Liu Y, Huang D L, Cheng M, Yang Y Y, Fu Y K, Luo H Z, Zhou Y. Sulfur doped carbon quantum dots loaded hollow tubular g-C_3N_4 as novel photocatalyst for destruction of *Escherichia coli* and tetracycline degradation under visible light. *Chemical Engineering Journal*, 2019, **378**: 122132
147. Li Y Y, Fang Y, Cao Z L, Li N J, Chen D Y, Xu Q F, Lu J M. Construction of g-C_3N_4/PDI@MOF heterojunctions for the highly efficient visible light-driven degradation of pharmaceutical and phenolic micropollutants. *Applied*

Catalysis B: Environmental, 2019, **250**: 150–162

148. Ren M L, Ao Y H, Wang P F, Wang C. Construction of silver/graphitic-C_3N_4/bismuth tantalate Z-scheme photocatalyst with enhanced visible-light-driven performance for sulfamethoxazole degradation. *Chemical Engineering Journal*, 2019, **378**: 122122
149. Shi W L, Liu C, Li M Y, Lin X, Guo F, Shi J. Fabrication of ternary $Ag_3PO_4/Co_3(PO_4)_2/g\text{-}C_3N_4$ heterostructure with following Type II and Z-Scheme dual pathways for enhanced visible-light photocatalytic activity. *Journal of Hazardous Materials*, 2020, **389**: 121907
150. Li Q Q, Zhao W L, Zhai Z C, Ren K X, Wang T Y, Guan H, Shi H F. 2D/2D $Bi_2MoO_6/g\text{-}C_3N_4$ S-scheme heterojunction photocatalyst with enhanced visible-light activity by Au loading. *Journal of Materials Science and Technology*, 2020, **56**: 216–226
151. Guo F, Huang X L, Chen Z H, Cao L W, Cheng X F, Chen L Z, Shi W L. Construction of $Cu_3P\text{-}ZnSnO_3\text{-}g\text{-}C_3N_4$ p-n-n heterojunction with multiple built-in electric fields for effectively boosting visible-light photocatalytic degradation of broad-spectrum antibiotics. *Separation and Purification Technology*, 2021, **265**: 118477
152. Fan G D, Ning R S, Yan Z S, Luo J, Du B H, Zhan J J, Liu L S, Zhang J. Double photoelectron-transfer mechanism in $Ag–AgCl/WO_3/g\text{-}C_3N_4$ photocatalyst with enhanced visible-light photocatalytic activity for trimethoprim degradation. *Journal of Hazardous Materials*, 2021, **403**: 123964
153. Li D G, Huang J X, Li R B, Chen P, Chen D N, Cai M X, Liu H J, Feng Y P, Lv W Y, Liu G G. Synthesis of a carbon dots modified $g\text{-}C_3N_4/SnO_2$ Z-scheme photocatalyst with superior photocatalytic activity for PPCPs degradation under visible light irradiation. *Journal of Hazardous Materials*, 2021, **401**: 123257
154. Zhao W, Li Y J, Zhao P S, Zhang L L, Dai B L, Xu J M, Huang H B, He Y L, Leung D Y C. Novel Z-scheme $Ag\text{-}C_3N_4/SnS_2$ plasmonic heterojunction photocatalyst for degradation of tetracycline and H_2 production. *Chemical Engineering Journal*, 2021, **405**: 126555
155. Liu C, Feng Y, Han Z T, Sun Y, Wang X Q, Zhang Q F, Zou Z G. Z-scheme N-doped $K_4Nb_6O_{17}/g\text{-}C_3N_4$ heterojunction with superior visible-light-driven photocatalytic activity for organic pollutant removal and hydrogen production. *Chinese Journal of Catalysis*, 2021, **42**(1): 164–174
156. Shi Y H, Li J S, Sun Y S, Wan D J, Wan H Y, Wang Y F. FeOOH coupling and nitrogen vacancies functionalized $g\text{-}C_3N_4$ heterojunction for efficient degradation of antibiotics: performance evaluation, active species evolution and mechanism insight. *Journal of Alloys and Compounds*, 2022, **903**: 163898
157. Liu H, Chen H W, Ding N. Visible light-based $Ag_3PO_4/g\text{-}C_3N_4@MoS_2$ for highly efficient degradation of 2-amino-4-acetylaminoanisole (AMA) from printing and dyeing wastewater. *International Journal of Environmental Research and Public Health*, 2022, **19**(5): 2934
158. Wang G H, Li Y J, Dai J L, Deng N S. Highly efficient photocatalytic oxidation of antibiotic ciprofloxacin using $TiO_2@g\text{-}C_3N_4@$biochar composite. *Environmental Science and Pollution Research International*, 2022, **29**(32): 48522–48538
159. Tan W K, Muto H, Kawamura G, Lockman Z, Matsuda A. Nanomaterial fabrication through the modification of sol–gel derived coatings. *Nanomaterials*, 2021, **11**(1): 181
160. Giampiccolo A, Tobaldi D M, Leonardi S G, Murdoch B J, Seabra M P, Ansell M P, Neri G, Ball R J. Sol gel graphene/TiO_2 nanoparticles for the photocatalytic-assisted sensing and abatement of NO_2. *Applied Catalysis B: Environmental*, 2019, **243**: 183–194
161. Rutkowska I, Marchewka J, Jeleń P, Odziomek M, Korpyś M, Paczkowska J, Sitarz M. Chemical and structural characterization of amorphous and crystalline alumina obtained by alternative sol–gel preparation routes. *Materials*, 2021, **14**(7): 1761
162. Ishikawa K, Garskaite E, Kareiva A. Sol–gel synthesis of calcium phosphate-based biomaterials—A review of environmentally benign, simple, and effective synthesis routes. *Journal of Sol-Gel Science and Technology*, 2020, **94**(3): 551–572
163. Pant B, Park M, Park S J. Recent advances in TiO_2 films prepared by sol-gel methods for photocatalytic degradation of organic pollutants and antibacterial activities. *Coatings*, 2019, **9**(10): 613
164. Manh N T, Thanh N T, Tam P D, Minh V T N, Thang C X, Pham V H. Synthesis of nano-urchin Mo-doped VO_2 particles by the hydrothermal method. *Journal of Applied Spectroscopy*, 2020, **87**(1): 22–25
165. Guo F, Bao L, Wang H, Larson S L, Ballard J H, Knotek-Smith H M, Zhang Q, Su Y, Wang X, Han F. A simple method for the synthesis of biochar nanodots using hydrothermal reactor. *MethodsX*, 2020, **7**: 101022
166. Yang L, Shen J N, Zhang W Y, Wu W P, Wei Z F, Chen M F, Yan J C, Qian L B, Han L, Li J, Gu M. Hydrothermally assisted synthesis of nano zero-valent iron encapsulated in biomass-derived carbon for peroxymonosulfate activation: the performance and mechanisms for efficient degradation of monochlorobenzene. *Science of the Total Environment*, 2022, **829**: 154645
167. Thirumal V, Yuvakkumar R, Kumar P S, Keerthana S P, Ravi G, Thambidurai M, Dang C, Velauthapillai D. Facile hydrothermal synthesis of MXene@antimony nanoneedle composites for toxic pollutants removal. *Environmental Research*, 2022, **210**: 112904
168. Liu S, Liu Y, Chen M, Li L, Tu W, Huang Z. $CuFe_2O_4$

modified expanded graphite synthesized by urea-assisted hydrothermal method for tetracycline treatment through persulfate activation: characterization, mechanism and degradation intermediates. *Chemical Engineering Journal*, 2022, **433**: 133516

169. Sun B, Tian Y, Feng M L, Zhang S H, Yang H, Qin J M, Bi W L, Qiao X, Liu F W, Hou Q J. A novel win–win wastewater treatment process: recover functional element from sludge to enhances TiO_2 for deep photocatalytic oxidation. *Chemical Engineering Journal*, 2025, **507**: 160627

170. Sun B, Guo Z Y, Ren F F, Pan X N, Lyu C J, Qiao X X, Bi W L, Liu F W, Hou Q J. Enhanced photocatalyst with TiO_2-anchored iron tailings structure for highly efficient degradation of doxycycline hydrochloride. *Journal of Cleaner Production*, 2023, **427**: 139241

171. Hu W J, Deng J. Photocatalytic decarboxylation of waste cooking oil for green and efficient biodiesel production and life cycle assessment. *Chemical Engineering Journal*, 2025, **519**: 164955